Smoothing traffic flow via control of autonomous vehicles

Yang Zheng,[1,2,*] Jiawei Wang,[2,3,†] and Keqiang Li[2,3,‡]

[1]*Department of Engineering Science, University of Oxford, Oxford, United Kingdom*

[2]*State Key Laboratory of Automotive Safety & Energy, Tsinghua University, Beijing, China*

[3]*Center for Intelligent Connected Vehicles & Transportation, Tsinghua University, Beijing, China*

The emergence of autonomous vehicles is expected to revolutionize road transportation in the near future. Although large-scale numerical simulations and small-scale experiments have shown promising results, a comprehensive theoretical understanding to smooth traffic flow via autonomous vehicles is lacking. Here, from a control-theoretic perspective, we establish analytical results on the controllability, stabilizability, and reachability of a mixed traffic system consisting of human-driven vehicles and autonomous vehicles in a ring road. We show that the mixed traffic system is not completely controllable, but is stabilizable, indicating that autonomous vehicles can not only suppress unstable traffic waves but also guide the traffic flow to a higher speed. Accordingly, we establish the maximum traffic speed achievable via controlling autonomous vehicles. We also design an optimal control strategy for autonomous vehicles to actively dampen undesirable perturbations. These theoretic findings validate the high potential of autonomous vehicles to smooth traffic flow.

Introduction

Modern societies are increasingly relying on complex road transportation systems to support our daily mobility needs. In particular big cities, the traffic demand is placing a heavy burden on the existing transportation infrastructures, sometimes leading to severely congested road networks [1]. Traffic congestion not only results in the loss of fuel economy and travel efficiency, but also increases the potential risk of traffic accidents and public health [2].

Understanding traffic dynamics is essential if we are to redesign infrastructures, or to guide/control transportation, to mitigate road congestions and smooth traffic flow [3, 4]. The subject of traffic dynamics has attracted research interest from many disciplines, including mathematics, physics, and engineering. Since the 1930s, a wide range of models at both the macroscopic and microscopic levels have been proposed to describe traffic behavior [3]. Based on these traffic models, many control methods have been introduced and implemented to improve the performance of road transportation systems [4]. Currently, most control strategies rely on actuators at fixed locations. For example, variable speed advisory or variable speed limits [5] are commonly implemented through traffic signs on roadside infrastructure, and ramp metering [6] typically relies on traffic signals located at the freeway entrances. These strategies are essentially external regulation methods imposed on traffic flow.

As a key ingredient of traffic flow, the motion of vehicles plays a fundamental role in road transportation systems. In the past decades, major car-manufacturers and technology companies have invested in developing vehicles with high levels of automation, and some prototypes of autonomous self-driving cars have been tested in real traffic environments [7]. The emergence of autonomous vehicles is expected to revolutionize road transportation. In particular,

*Electronic address: yang.zheng@eng.ox.ac.uk

†Electronic address: wang-jw18@mails.tsinghua.edu.cn

‡Electronic address: likq@tsinghua.edu.cn

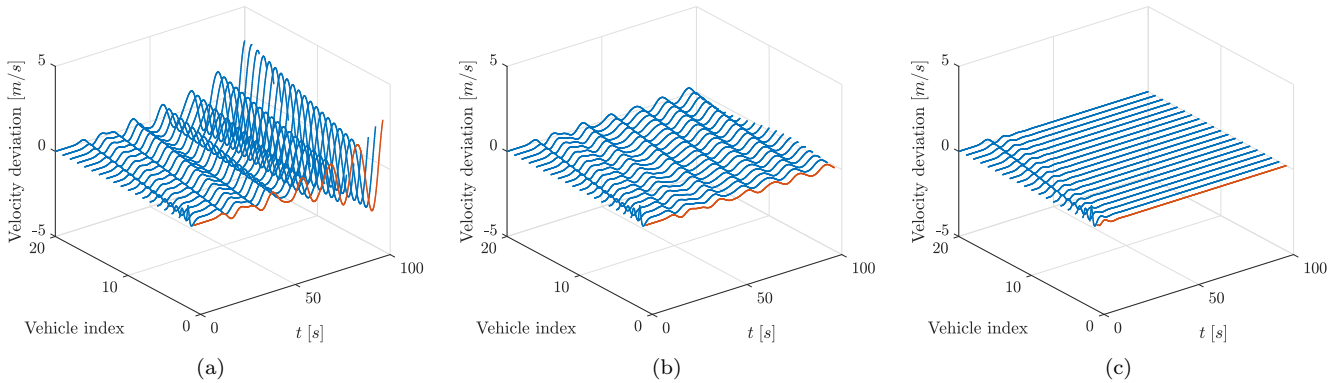

Figure 1: Response profiles to an impulse perturbation in traffic systems on a ring road. Vehicle no.2 has an initial perturbation, and the parameters of human-driven vehicles are chosen to resemble the wave behavior in the real-world experiment [23]. (a) All the vehicles are human-driven, where the perturbation is amplified and stop-and go waves will appear accordingly. (b) Vehicle no.1 is a CACC-equipped vehicle which adjusts its behavior passively according to its direct preceding vehicle. In this case, the perturbation is not amplified but small traffic waves still persist for a long period. (c) Vehicle no.1 adopts an optimal control strategy considering the global behavior of the entire mixed traffic flow to mitigate undesirable perturbations actively. In this case, the perturbation is attenuated, and the traffic flow becomes smooth quickly.

the advancements of autonomous vehicles offer new opportunities for traffic control, where autonomous vehicles can act as moving actuators to influence traffic flow internally. Most research on the control of traffic flow via autonomous vehicles has focused on platooning of a series of adjacent vehicles or cooperative adaptive cruise control (CACC) [8, 9]. In the context of platoon control, all involved vehicles are assumed to be autonomous and can be controlled to maintain a string stable platoon, such that disturbances along the platoon are dissipated. Significant theoretical and practical advances have been made in designing sophisticated controllers at the platoon level [10–12]. While traffic systems with fully autonomous vehicles may be of great interest in the far future, the near future will have to meet a mixed traffic where both autonomous and human-driven vehicles exist. In fact, early autonomous vehicles need to cooperate in traffic systems where most vehicles are human-driven. This situation is more challenging in terms of theoretical modeling and stability analysis, and many existing studies are based on numerical simulations [13–15]. One recent concept is the connected cruise control that considers mixed traffic scenarios where autonomous vehicles can use the information from multiple human-driven vehicles ahead to make control decisions [16, 17]. More recently, Cui *et al.* first pointed out the potential of a single autonomous vehicle in stabilizing mixed traffic flow [18], and they also implemented simple control strategies to demonstrate the dissipation of stop-and-go waves via a single autonomous vehicle in real experiments [19]. The control principle is essentially a slow-in fast-out approach, which is an intuitive method to dampen traffic jams [20]. More sophisticated strategies, such as deep reinforcement learning, have also recently been investigated to improve traffic flow in mixed traffic scenarios via numerical simulations [21, 22].

While the potential of autonomous vehicles has been recognized and demonstrated [18, 19, 21, 22], a comprehensive theoretical understanding is lacking. In this paper, we provide a theoretical analysis on the potential of autonomous vehicles in smoothing mixed traffic flow from a complex system viewpoint. In principle, the behavior of traffic flow emerges from the collective dynamics of many individual human-driven and/or autonomous vehicles [3], where autonomous vehicles can serve as controllable nodes. In the area of complex systems, controlling the collective behavior of dynamical agents interacting over networks has a long history, capturing phenomena from flocking of birds or fish to the synchronization of coupled oscillators [24–26]. From a complex system perspective, we first investigate analytical

stability results for traffic systems with only human-driven vehicles. After introducing an autonomous vehicle as a controllable node, we next establish basic notions of controllability and stabilizability of such mixed traffic flow. These theoretical results reveal the high potential of autonomous vehicles to guide the collective dynamics of mixed traffic flow to a desired state (*e.g.*, a higher traffic speed). Accordingly, we design an optimal control strategy of autonomous vehicles to smooth mixed traffic flow. Instead of responding to traffic perturbations passively, the proposed optimal control strategy considers the global behavior of the entire mixed traffic flow to mitigate undesirable perturbations actively (see Figure 1 for illustration). Extensive numerical experiments validate our theoretical analysis and clearly demonstrates the high potential of autonomous vehicles on controlling and smoothing traffic flow.

Results

Theoretical framework of mixed traffic systems. We consider a single-lane ring road of length L and with n vehicles. As discussed in Cui *et al.* [18], the ring road setting has several theoretical advantages for modeling a traffic system, including 1) the existence of experiment results that can be used to calibrate model parameters [23], 2) perfect control of average traffic density, and 3) correspondence with an infinite straight road with periodic traffic dynamics. We denote the position of the i-th vehicle as $p_i(t)$ along the ring road, and its velocity is denoted as $v_i(t) = \dot{p}_i(t)$. The spacing of vehicle i, *i.e.*, the distance between two adjacent vehicles, is defined as $s_i(t) = p_{i-1}(t) - p_i(t)$. Note that we ignore the vehicle length without loss of generality. For simplicity, we assume that there is one autonomous vehicle and the rest are human-driven vehicles. The autonomous vehicle is indexed as no. 1. The scenario with multiple autonomous vehicles will be discussed at the end of this section.

Real-world human car-following behaviors are typically modeled by nonlinear processes [3, 4] $\dot{v}_i(t) = F(s_i(t), \dot{s}_i(t), v_i(t))$, but stability analysis around an equilibrium point can be performed via a linearization [27]. From a global complex system viewpoint, we arrive at the following canonical linear dynamics (see Methods)

$$\dot{x}(t) = Ax(t) + Bu(t), \tag{1}$$

where $u(t) \in \mathbb{R}$ denotes the control input of the autonomous vehicle on the traffic system dynamics; the vector $x(t) = \left[x_1^\mathsf{T}(t), x_2^\mathsf{T}(t), \ldots, x_n^\mathsf{T}(t)\right]^\mathsf{T} \in \mathbb{R}^{2n}$ captures the error state of n vehicles at time t; the error state of vehicle i is defined as $x_i(t) = \left[s_i(t) - s^*, v_i(t) - v^*\right]^\mathsf{T}$ with s^*, v^* being the equilibrium spacing and velocity of each human-driven vehicle, $i = 2, \ldots, n$, and $x_1(t) = \left[s_1(t) - s_c^*, v_1(t) - v^*\right]^\mathsf{T}$ denotes the error state of the autonomous vehicle with s_c^* being a tunable spacing. Note that for human-driven vehicles, the equilibrium traffic state (s^*, v^*) satisfies $F(s^*, 0, v^*) = 0$, which implies a certain relationship between the equilibrium spacing and equilibrium velocity (see Supplementary Note 1). Considering the ring road setting of mixed traffic systems, the matrices A and B in (1) are

$$A = \begin{bmatrix} C_1 & 0 & \ldots & \ldots & 0 & C_2 \\ A_2 & A_1 & 0 & \ldots & \ldots & 0 \\ 0 & A_2 & A_1 & 0 & \ldots & 0 \\ \vdots & \ddots & \ddots & \ddots & \ddots & \vdots \\ 0 & \ldots & 0 & A_2 & A_1 & 0 \\ 0 & \ldots & \ldots & 0 & A_2 & A_1 \end{bmatrix}, B = \begin{bmatrix} B_1 \\ B_2 \\ B_2 \\ \vdots \\ B_2 \end{bmatrix}, \tag{2}$$

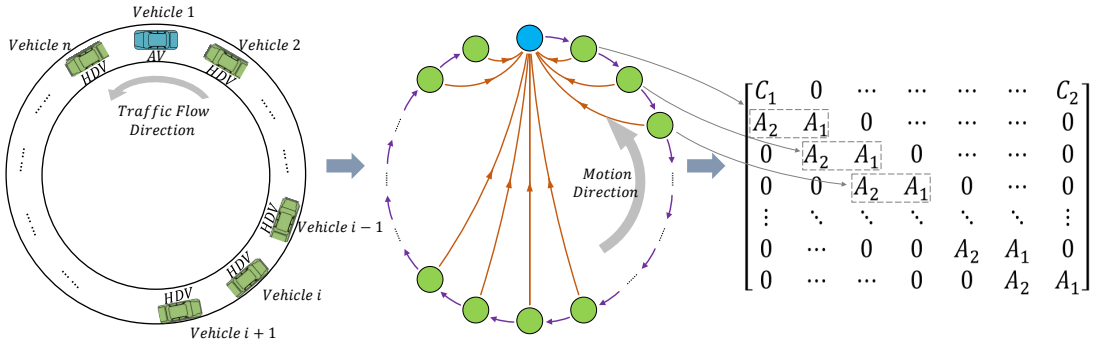

Figure 2: Model establishment schematic, AV: autonomous vehicle; HDV: human-driven vehicle. (a) The ring road traffic scenario that includes one autonomous vehicle (blue) and $n-1$ human-driven vehicles (green). (b) A simplified network system schematic. Purple arrows indicate the interaction between adjacent vehicles, meaning that each human-driven vehicle considers the state of its preceding vehicle only. Orange arrows show the information flow of the whole system, assuming that the traffic state is observable to the autonomous vehicle. (c) The system matrix A of the mixed traffic dynamics, as shown in (2).

where each block matrix is given by

$$A_1 = \begin{bmatrix} 0 & -1 \\ \alpha_1 & -\alpha_2 \end{bmatrix}, \; A_2 = \begin{bmatrix} 0 & 1 \\ 0 & \alpha_3 \end{bmatrix}, \; C_1 = \begin{bmatrix} 0 & -1 \\ 0 & 0 \end{bmatrix}, \; C_2 = \begin{bmatrix} 0 & 1 \\ 0 & 0 \end{bmatrix}, \; B_1 = \begin{bmatrix} 0 \\ 1 \end{bmatrix}, \; B_2 = \begin{bmatrix} 0 \\ 0 \end{bmatrix}, \tag{3}$$

with parameters $\alpha_1 = \frac{\partial F}{\partial s}, \alpha_2 = \frac{\partial F}{\partial \dot{s}} - \frac{\partial F}{\partial v}, \alpha_3 = \frac{\partial F}{\partial \dot{s}}$ evaluated at the equilibrium state (s^*, v^*). Considering the real driver behavior, we should have $\alpha_1 > 0$, $\alpha_2 > 0$ and $\alpha_3 > 0$. It can be shown that ring road traffic with common car-following dynamics can be linearized into the form of (1)—(3) (see Supplementary Note 1). In (1), the evolution of each vehicle's state is determined by its own state and the state of its direct preceding vehicle only; see Figure 2 for a schematic model. In the following, we provide a theoretical analysis on the potential of the autonomous vehicle on smoothing the mixed traffic flow and design an optimal control input $u(t)$ for the autonomous vehicle.

Stability of traffic systems with human-driven vehicles only. If all the vehicles are driven by human, the traffic system dynamics (1) can be simplified into

$$\dot{x}(t) = \hat{A}x(t), \tag{4}$$

where

$$\hat{A} = \begin{bmatrix} A_1 & 0 & \dots & \dots & 0 & A_2 \\ A_2 & A_1 & 0 & \dots & \dots & 0 \\ 0 & A_2 & A_1 & 0 & \dots & 0 \\ \vdots & \ddots & \ddots & \ddots & \ddots & \vdots \\ 0 & \dots & 0 & A_2 & A_1 & 0 \\ 0 & \dots & \dots & 0 & A_2 & A_1 \end{bmatrix}.$$

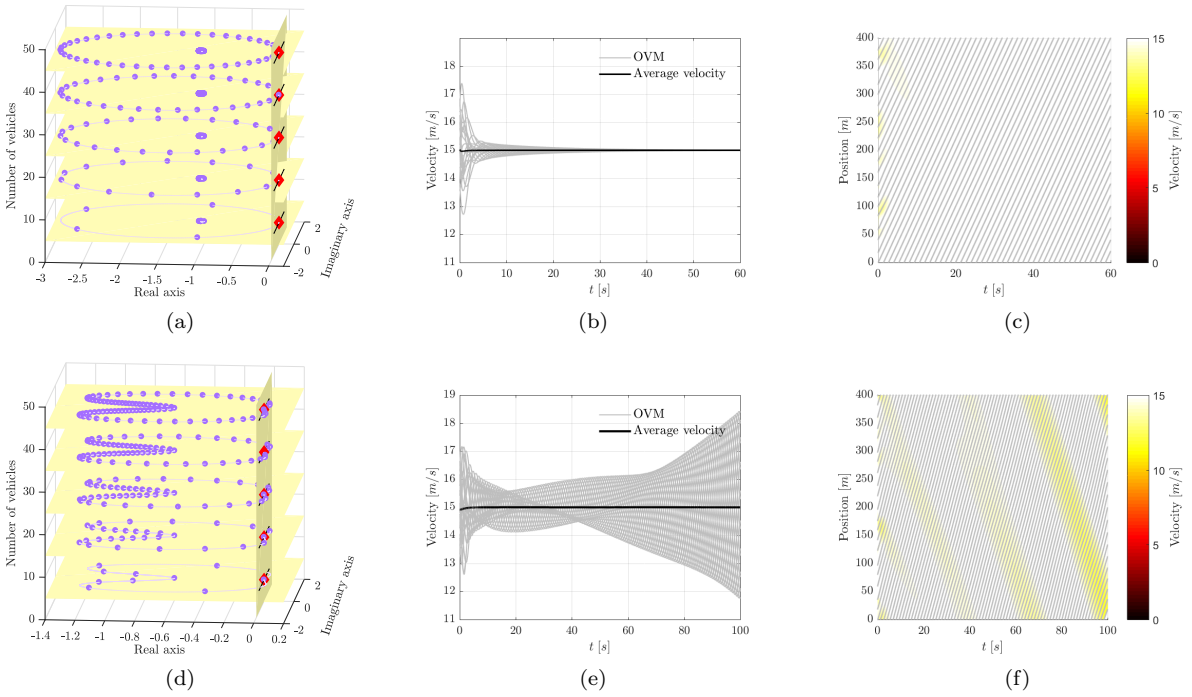

Figure 3: Response profiles to a random initial perturbation in traffic systems on a ring road. (a) Eigenvalue distribution for different n when $\alpha = 1.0, \beta = 1.5$ in the OVM model. In this case, the stability criterion (5) is satisfied. A zero eigenvalue (red diamond) always exists irrespectively of n and the rest eigenvalues have negative real parts. (b)-(c) Time-domain simulations corresponding to the stable traffic system in (a) with $n = 20$. All the vehicles have a random initial perturbation from equilibrium, and the perturbation vanishes as the traffic system evolves. (d) Eigenvalue distribution for different n when $\alpha = 0.6, \beta = 0.9$ in the OVM model. In this case, the stability criterion (5) is not satisfied. A zero eigenvalue (red diamond) exists and some eigenvalues have positive real parts when n increases, indicating that the traffic system becomes unstable. (e)-(f) Time-domain simulations corresponding to the unstable traffic system in (d) with $n = 20$, where the traffic wave persists and is amplified.

Since $\hat{A}$ is block circulant, it can be diagonalized into a block diagonal matrix [28, 29] where each block is of size two. Then, we can show that there always exists a zero eigenvalue which corresponds to the ring road structure, indicating a constant value in the system evolution (see Methods). In addition, from the block diagonalization, we can derive the following analytical criterion for the other eigenvalues to have negative real parts, which guarantees stability of the traffic system (4) with any finite n (*i.e.*, small perturbations will be attenuated in the system evolution)

$$\alpha_2^2 - \alpha_3^2 - 2\alpha_1 \geq 0. \tag{5}$$

This result is consistent with the result in [18] where frequency analysis was used. The optimal-velocity model (OVM) is widely-used to describe human car-following dynamics (see Supplementary Note 1), and is given by $F(s_i(t), \dot{s}_i(t), v_i(t)) = \alpha(V(s_i(t)) - v_i(t)) + \beta\dot{s}_i(t)$, where α and β represent the driver's sensitivity to velocity errors and $V(s)$ denotes an optimal velocity function according to the spacing $s_i(t)$ [30]. For this car-following model, the stability criterion (5) is reduced to $\alpha + 2\beta \geq \dot{V}(s^*)$. To guarantee stability, this inequality indicates that human drivers should have a quicker response to velocity deviations than the sensitivity of the optimal velocity function with respect to spacing in the equilibrium; otherwise, the traffic system may become unstable and small perturbations would cause stop-and-go waves; see Figure 3 for an illustration of stable and unstable traffic systems.

Controllability and stabilizability of mixed traffic systems. It is revealed that a traffic system with human-driven vehicles may be unstable and stop-and-go waves occur accordingly. Here, we address the potential of autonomous vehicles to suppress the instability of mixed traffic flow. Specifically, we consider two fundamental concepts, controllability and stabilizability, of the mixed traffic system (1).

According to control theory, the controllability of a dynamical system captures the ability to guide the system's behavior towards a desired state using appropriate control inputs, and the system is stabilizable if all uncontrollable modes are stable [31]. Precisely, the linearized mixed traffic system (1) is controllable if and only if the controllability matrix $Q_{\mathrm{c}} = \begin{bmatrix} B & AB & A^2B & \dots & A^{2n-1}B \end{bmatrix}$ has full rank. As explained in the Methods, we prove that the mixed traffic system is not completely controllable and there always exists at least one uncontrollable mode. Precisely, we prove that

$$\mathrm{rank}(Q_{\mathrm{c}}) = \begin{cases} 2n-1, & \text{if } \alpha_1 - \alpha_2\alpha_3 + \alpha_3^2 \neq 0, \\ n, & \text{if } \alpha_1 - \alpha_2\alpha_3 + \alpha_3^2 = 0. \end{cases} \tag{6}$$

Furthermore, irrespectively of the values of $\alpha_1, \alpha_2, \alpha_3$, we show that one uncontrollable component exactly corresponds to the sum of each vehicle's spacing, which remains a constant value during the system evolution and is determined by the ring road circumference (see Supplementary Note 3). In other words, this uncontrollable mode corresponds to a zero eigenvalue. When $\alpha_1 - \alpha_2\alpha_3 + \alpha_3^2 \neq 0$, the rest of modes are all controllable, and if $\alpha_1 - \alpha_2\alpha_3 + \alpha_3^2 = 0$, the rest of modes are all stable considering the stability test (5). Therefore, the mixed traffic system (1) is always stabilizable when there exists a single autonomous vehicle in the system.

Consequently, by choosing an appropriate control input, the autonomous vehicle can not only stabilize the global traffic flow, but also steer the system to a higher equilibrium traffic speed (a detailed analysis is presented in the next section). Numerical simulations in Figure 4 confirms our analysis, where the previous unstable traffic system with human-driven vehicles only (Figure 3(e)) becomes stable (Figure 4(a)), and the traffic speed can be increased from 15 m/s to 16 m/s (Figure 4(b)).

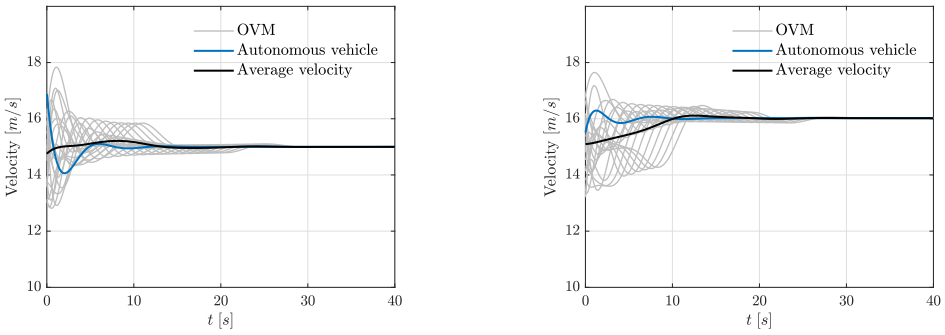

Figure 4: Stabilizing traffic flow and increasing traffic speed. The scenario is the same as that in Figure 3(e), where the traffic system with human-driven vehicles only is unstable. (a) The mixed traffic system becomes stable after introducing an autonomous vehicle with an appropriate control strategy. (b) The traffic flow can be guided to a higher stable velocity via controlling the autonomous vehicle.

Reachability and system final state. We have shown that the mixed traffic system (1) is always stabilizable when there exists an autonomous vehicle. In fact, we can further predict the system final state, which sheds some insight on the reachability of the equilibrium traffic state (s^*, v^*). Also, it is explicitly shown that the autonomous vehicle can indeed increase traffic equilibrium speed v^*.

Recall that we can design the desired spacing s_c^* for the autonomous vehicle. We assume a linear state feedback controller $u(t) = -Kx(t)$, where $K = \left[k_{1,1}, k_{1,2}, k_{2,1}, k_{2,2,}, \ldots, k_{n,1}, k_{n,2}\right] \in \mathbb{R}^{1\times 2n}$ is the feedback gain. As explained in the Methods, we prove that irrespectively of the initial state $x(0)$, the final state of the stable mixed traffic system must be in the following form:

$$\left[s_c^* + s_e, v^* + v_e, s^* + \frac{\alpha_2 - \alpha_3}{\alpha_1} v_e, v^* + v_e, \ldots, s^* + \frac{\alpha_2 - \alpha_3}{\alpha_1} v_e, v^* + v_e\right]^{\mathsf{T}} \in \mathbb{R}^{2n},$$

where s_e and v_e are the solution of (7).

$$\left(\frac{\alpha_2 - \alpha_3}{\alpha_1} \Sigma_{i=2}^n k_{i,1} + \Sigma_{i=1}^n k_{i,2}\right) v_e + k_{1,1} s_e = 0, \tag{7a}$$

$$(n-1)\left(\frac{\alpha_2 - \alpha_3}{\alpha_1} v_e + s^*\right) + s_e + s_c^* = L, \tag{7b}$$

where $\alpha_1, \alpha_2, \alpha_3$ are the parameters in car-following dynamics (3), and $k_{i,1}, k_{i,2}$ are fixed feedback gains of the autonomous vehicle. Indeed, equation (7b) exactly corresponds to the uncontrollable mode, showing that the sum of each vehicle's spacing is constant, as discussed in the previous section. To reach the desired equilibrium state (s^*, v^*), we should have $s_e = 0$ and $v_e = 0$, and this leads to the tunable spacing of the autonomous vehicle, *i.e.*, $s_c^* = L - (n-1)s^*$. Under this choice, the final reachable traffic state is

$$\left[L - (n-1)s^*, v^*, s^*, v^*, \ldots, s^*, v^*\right]^{\mathsf{T}} \in \mathbb{R}^{2n}.$$

In principle, since the mixed traffic system (1) is stabilizable, it can be guided to reach any equilibrium state with traffic speed v^* via controlling the autonomous vehicle properly. In practice, however, the spacing of the autonomous vehicle cannot be negative, *i.e.*, $s_c^* > 0$, which is equivalent to

$$(s^*)_{\max} < \frac{L}{n-1}, \tag{8}$$

This sets up a maximum equilibrium traffic speed v^* according to $F(s^*, 0, v^*) = 0$ (see Supplementary Figure S1 for a typical relationship between s^* and v^*), which is higher than the equilibrium traffic speed with only human-driven vehicles. A physical interpretation is that the autonomous vehicle can follow its preceding vehicle at a shorter distance and leave more space for its following human-driven vehicles, which in turn triggers the human-driven vehicles to travel at a higher speed in the equilibrium; see Supplementary Figure S2 for illustration.

Designing an optimal control strategy. We have shown that a mixed traffic system with a single autonomous vehicle is stabilizable. Following standard control theory [31], we can design an optimal control strategy to reject perturbations in the mixed traffic system. This scenario is modeled by assuming that there exists a disturbance signal

$w_i(t)$ in each vehicle's acceleration signal. In other words, the linearized dynamics of human-driven vehicle (1) become $\dot{x}_i(t) = A_1 x_i(t) + A_2 x_{i-1}(t) + H_1 w_i(t)$ with $H_1 = \begin{bmatrix} 0, 1 \end{bmatrix}^\mathsf{T}$. Then, we design an optimal control input $u(t) = -Kx(t)$ to minimize the influence of disturbances on the traffic system. Mathematically, we aim to solve an optimization problem $\min_K \|G_{wz}\|$, where G_{wz} denotes the transfer function from disturbance signal $w(t) = \begin{bmatrix} w_1(t), \ldots, w_n(t) \end{bmatrix}^\mathsf{T}$ to the traffic performance state $z(t) = \begin{bmatrix} \gamma_s \tilde{s}_1(t), \gamma_v \tilde{v}_1(t), \ldots, \gamma_s \tilde{s}_n(t), \gamma_v \tilde{v}_n(t), \gamma_u u(t) \end{bmatrix}^\mathsf{T}$ with positive weights $\gamma_s > 0, \gamma_v > 0, \gamma_u > 0$, and $\|\cdot\|$ denotes the $\mathcal{H}_2$ norm of a transfer function that captures the influence of disturbances. The weights $\gamma_s, \gamma_v, \gamma_u$ represent the penalties of position deviations, velocity deviations, and control energy, respectively. It is known that this optimization problem is tractable [31], and can be solved via existing solvers (see Supplementary Note 4).

Numerical experiments of smoothing traffic flow via a single autonomous vehicle. Figure 1 and Figure 4 have demonstrated the ability of a single autonomous vehicle to smooth the traffic flow where there exist weak perturbations. Here, we consider a scenario with the presence of infrastructure bottlenecks or lane changing [19], where one vehicle has a rapid deceleration representing a strong perturbation. In the beginning, the traffic flow is at the equilibrium state with the velocity $15m/s$. And then at $t = 20s$, the i-th vehicle decelerates to $5m/s$ in two seconds. As shown in Figure 5, we observe that if all the vehicles are human-driven, the perturbation may grow stronger during the propagation process, while the autonomous vehicle with an optimal control strategy can respond actively to attenuate the perturbation and stabilize the traffic flow. In Supplementary Note 5, we present the numerical results for the scenarios with different positions of the perturbation, *i.e.*, the perturbation appears at vehicle $2, 3, \ldots, n$, respectively. We also compare the optimal control strategy and two other heuristic strategies (FollowerStopper and PI with Saturation [19]). Numerical experiments confirm that the optimal control method has the best performance in terms of control energy and settling time (see Supplementary Note 5).

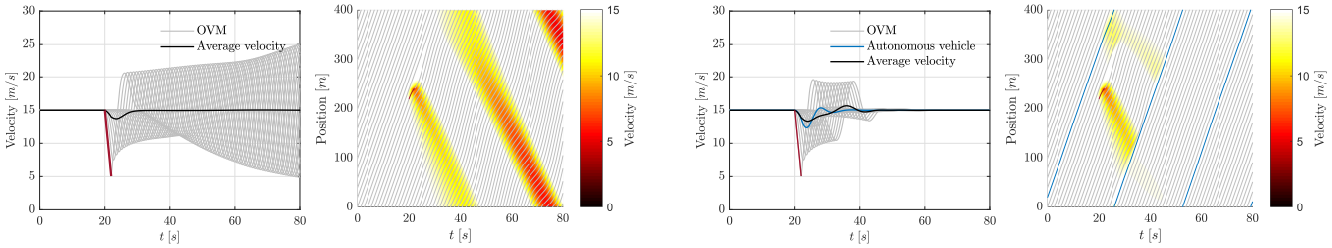

(a) (b)

Figure 5: Numerical results for the scenario with a rapid and strong perturbation in the 6-th vehicle. (a) The traffic system consists of human-driven vehicles only. (b) The mixed traffic system has an autonomous vehicle that adopts the optimal control strategy. In panel (a) or (b), the right figure shows the vehicles' trajectories, where the red zone represents the traffic wave; the left figure shows the vehicles' velocities, where the red line denotes the perturbation and the black line is the average velocity of all vehicles.

Traffic systems with multiple autonomous vehicles. The mixed traffic system with a single autonomous vehicle is stabilizable, which is independent of the number of vehicles n. Also, an optimal control strategy $u(t)$ can be obtained by solving an optimization problem. However, it might be not practical to control a mixed traffic system consisting of many human-driven vehicles and a single autonomous vehicle. Under this circumstance, the energy and time required

for attenuating disturbances may be large, even when the autonomous vehicle adopts the optimal control strategy. Figure 6 shows the control energy $\int_0^\infty u^\mathsf{T} u dt$ of the autonomous vehicle and time required for attenuating an impulse disturbance, both of which grow almost linearly as the number of human-driven vehicles increases. This limitation motivates an investigation on the potential of multiple autonomous vehicles to smooth traffic flow.

Indeed, our previous analysis can be extended to a mixed traffic system with multiple autonomous vehicles. Specifically, we assume that there are n vehicles in the traffic flow with k autonomous vehicles ($k < n$). As explained in the Supplementary Note 6, similarly to system (1), there exists an uncontrollable mode in the mixed traffic system with k autonomous vehicles. As expected, the mixed traffic system with k autonomous vehicles is stabilizable. In addition, we can show that the reachable final traffic state is

$$\left[s_{1,c}^*, v^*, s^*, v^*, \ldots, s_{k,c}^*, v^*, \ldots, s^*, v^*\right]^\mathsf{T} \in \mathbb{R}^{2n}.$$

with $\Sigma_{j=1}^k s_{j,c}^* = L - (N-k)s^*$, where $s_{j,c}^*, j = 1, \ldots, k$ denotes the desired spacing of the j-th autonomous vehicle. In this case, the maximum spacing for each human-driven vehicle in the equilibrium can be increased to

$$(s^*)_{\max} < \frac{L}{n-k},$$

and this corresponds to a higher equilibrium traffic velocity v^*. We conduct numerical experiments for the scenario where the traffic system has two autonomous vehicles, and the results are shown in Figure 6. It is clear that both the settling time and the control energy of each autonomous vehicle decrease by a factor of two approximately, when there are two autonomous vehicles in the traffic system uniformly. Based on the results, we may estimate the market penetration rate of autonomous vehicles to control traffic flow effectively when adopting the optimal control strategy. In the scenario of Figure 6, if one wants to reject the influence of the perturbation on traffic flow within 30 seconds, a single autonomous vehicle can control the traffic flow consisting of around 20 human-driven vehicles. This number agrees with the results from real-world experiments [19].

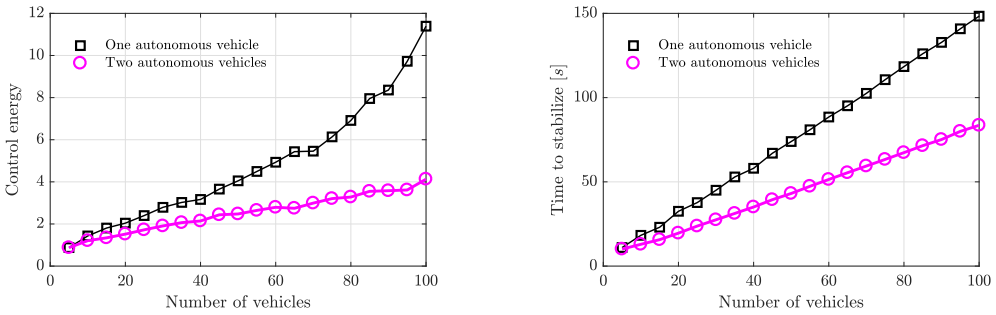

Figure 6: Simulation results at different system scales. We ran 2000 random simulations for each value of n. The parameters are as follows: $\gamma_s = 0.03$, $\gamma_v = 0.15$, $\gamma_u = 1$. (a) The control energy $\int_0^\infty u^\mathsf{T} u dt$ needed to stabilize the traffic flow for each autonomous vehicle. (b) The time required to stabilize the traffic system.

Discussion

As demonstrated in the pioneering experiments in [19], unlike the traditional control methods that regulate traffic flow externally at fixed positions, autonomous vehicles can be used as moving actuators to control traffic flow internally. In this paper, we have introduced a comprehensive theoretical analysis to address the potential of autonomous vehicles on smoothing mixed traffic flow. Specifically, we have derived the criterion of stability for traffic systems with human-driven vehicles only, and analyzed the controllability, stabilizability, and reachability of mixed traffic systems. Also, an optimal control strategy has been introduced to actively smooth mixed traffic flow.

From our analysis, we pointed out that the mixed traffic system is stabilizable, and is not completely controllable. Through controlling the autonomous vehicle properly, the entire traffic system can be guided to a desired traffic state. In particular, the desired equilibrium state (s^*, v^*) can be designed to vary within a certain range. The setting is similar to the design of vehicle platoons, where all autonomous vehicles can be controlled to reach a desired spacing and a desired velocity [10–12]. In a mixed traffic system, the desired state (s^*, v^*) for human-driven vehicles should satisfy the car-following models (see Supplementary Figure 1), while the desired state (s_c^*, v^*) for the autonomous vehicle can be designed separately. This leads to the reachability result, where we have shown a single autonomous vehicle can not only smooth traffic flow but also increase traffic speed. In our framework, we have proposed that the autonomous vehicle can respond to external perturbations actively to smooth traffic flow efficiently. For this objective, we computed an optimal control strategy by solving an optimization problem that considers the entire traffic state. The resulting controller can smooth the traffic flow more quickly than traditional passive control strategies [18, 19] (See Figure 1). Note that in the design of optimal control strategies, we can choose three parameters, corresponding to the spacing deviation γ_s, velocity deviation γ_v and the control energy penalty γ_u. These three parameters can be adjusted depending on different preferences. In addition, we have shown that controlling multiple autonomous vehicles has better performance for large-scale mixed traffic systems. Autonomous vehicles can cooperate with each other to reduce the time and energy for attenuating perturbations and smoothing traffic flow. In our framework, it is possible to identify an appropriate market penetration rate of autonomous vehicles from the perspective of settling time. Based on our simulations, autonomous vehicles have practical ability to smooth traffic flow at a low penetration rate (one autonomous vehicles per around 20 human-driven vehicles) when adopting the optimal control strategy. The ability of autonomous vehicles at a low penetration rate has been experimentally confirmed in [19].

A few other topics are worth further investigation. In our current analysis, we have assumed autonomous vehicles have access to the global the traffic state, *i.e.*, the information of all other human-driven vehicles. Due to the limit of communication ranges, autonomous vehicles may be only able to obtain the information of its neighboring vehicles. It is interesting to design a localized optimal controller, and this leads to the notion of structured controller synthesis [32, 33]. For the tractable issue in theory, we have assumed homogeneous dynamics for human-driven vehicles, and potential time delays are ignored. One interesting direction is to consider heterogeneity and time delay in controlling mixed traffic systems. We note that some recent work has considered the effect of heterogeneity and time delays at the level of platoon control [34–36], which may offer some insights for the controller design in mixed traffic systems as well. Finally, our current analysis focused on the single-lane ring road setting, and it would be interesting to extend our analysis to the scenarios with multiple lanes and lane-changing behavior.

Methods

Deriving the mathematical model of mixed traffic system. Using the first-order Taylor expansion, the general car-following model of human-driven vehicles, *i.e.*, $\dot{v}_i(t) = F(s_i(t), \dot{s}_i(t), v_i(t)), i = 2, \ldots, n$, can be linearized into

$$\begin{cases} \dot{\tilde{s}}_i = \tilde{v}_{i-1}(t) - \tilde{v}_i(t), \\ \dot{\tilde{v}}_i = \alpha_1 \tilde{s}_i(t) - \alpha_2 \tilde{v}_i(t) + \alpha_3 \tilde{v}_{i-1}(t), \end{cases} \tag{9}$$

where $\tilde{s}_i(t) = s_i(t) - s^*, \tilde{v}_{\ i}(t) = v_i(t) - v^*$ and (s^*, v^*) denote the equilibrium traffic state. The kinetic model of the autonomous vehicle is given by

$$\begin{cases} \dot{\tilde{s}}_1 = \tilde{v}_n(t) - \tilde{v}_1(t), \\ \dot{\tilde{v}}_1 = u(t). \end{cases} \tag{10}$$

Combining (9) with (10) leads to the global linear dynamics (1). In Supplementary Note 1, we provide a detailed derivation of (1) as well as the linearization process for two typical car-following models (*i.e.*, OVM and IDM).

Deriving the Stability criterion. To analyze the stability of matrix $\hat{A}$, it is necessary and sufficient to study its eigenvalues' distribution. Since $\hat{A}$ is a block circulant matrix, it can be diagonalized to simplify the eigenvalue calculation. Define $\omega = e^{\frac{2\pi j}{n}}$, where $j = \sqrt{-1}$ denotes the imaginary unit, and the Fourier matrix F_n is defined as [28, 29]

$$F_n^* = \frac{1}{\sqrt{n}} \begin{bmatrix} 1 & 1 & 1 & \ldots & 1 \\ 1 & \omega & \omega^2 & \ldots & \omega^{n-1} \\ 1 & \omega^2 & \omega^4 & \ldots & \omega^{2(n-1)} \\ \vdots & \vdots & \vdots & & \vdots \\ 1 & \omega^{n-1} & \omega^{2(n-1)} & \ldots & \omega^{(n-1)(n-1)} \end{bmatrix},$$

where F_n^* denotes the conjugate transpose matrix of F_n. By the definition of Fourier matrix, we know that F_n and F_n^* are symmetric, *i.e.*, $F_n^* = (F_n^*)^{\mathsf{T}}$, $F_n = F_n^{\mathsf{T}}$, and that F_n is a unitary matrix, *i.e.*, $F_n F_n^* = I_n$, where I_n denotes the $n \times n$ identity matrix. Then, $\hat{A}$ can be diagonalized into

$$\hat{A} = (F_n^* \otimes I_2) \cdot \mathrm{diag}(D_1, D_2, \ldots, D_n) \cdot (F_n \otimes I_2),$$

where $\otimes$ denotes the Kronecker product, $D_i = A_1 + A_2\omega^{(n-1)(i-1)}, i = 1, 2, \ldots, n$, and $\mathrm{diag}(D_1, D_2, \ldots, D_n)$ denotes a block-diagonal matrix with $D_1, D_2, \ldots, D_n$ on its diagonal blocks. Then the eigenvalue λ satisfies

$$\begin{aligned}\det(\lambda I - A) &= \det(\lambda I - \mathrm{diag}(D_1, D_2, \ldots, D_n)) = \prod_{i=1}^{n} \det(\lambda I - D_i) \\ &= \prod_{i=1}^{n} \left(\lambda^2 + \left(\alpha_2 - \alpha_3\omega^{(n-1)(i-1)}\right)\lambda + \alpha_1\left(1 - \omega^{(n-1)(i-1)}\right)\right) \\ &= 0.\end{aligned} \tag{11}$$

Substituting the expression of ω into (11) leads to

$$e^{\frac{i-1}{n}\cdot 2\pi j} = \frac{\alpha_1 + \alpha_3\lambda}{\alpha_1 + \alpha_2\lambda + \lambda^2} = H(\lambda), \quad i = 1, 2, \ldots, n, \tag{12}$$

where $e^{\frac{i-1}{n}\cdot 2\pi j}, i = 1, \ldots, n$ are the complex roots of $z^n = 1$. It means for all $2n$ values of λ, the values of $H(\lambda)$ constitute n unit roots. When n or i changes, $H(\lambda)$ corresponds to different unit roots. Then, the condition that the roots of $|H(\lambda)| = 1$ have negative real parts is sufficient to guarantee that the zeros of (11) lie in the left half plane, *i.e.*, the system matrix $\hat{A}$ is stable. Following the strategy in [18], we arrive at the stability condition (5). The interested reader is referred to Supplementary Note 2 for details.

Controllability analysis via block circulant matrix diagonalization. For notational simplicity, we use a pair of matrices (A, B) to represent a linear system in the canonical form (1). First, we convert (A, B) into $(\hat{A}, B)$ by using a virtual control input $\hat{u}(t)$, defined as $\hat{u}(t) = u(t) - (\alpha_1\tilde{s}_1(t) - \alpha_2\tilde{v}_1(t) + \alpha_3\tilde{v}_n(t))$. This virtual control input can be viewed as the difference between the actual control value and the acceleration value when the vehicle is human-driven. Note that the controllability of a linear systems remains unchanged under feedback and linear transformations (see Supplementary Note 3), thus the controllability of (A, B) is the same as that of $(\hat{A}, B)$.

Next, we utilize $F_n^* \otimes I_2$ to transform $(\hat{A}, B)$ into $(\widetilde{A}, \widetilde{B})$, where $\widetilde{A} = (F_n^* \otimes I_2)^{-1}\hat{A}(F_n^* \otimes I_2)$ and $\widetilde{B} = (F_n^* \otimes I_2)^{-1}B$. In the state-space formulation, the new system $(\widetilde{A}, \widetilde{B})$ is of the following form

$$\dot{\tilde{x}} = \widetilde{A}\tilde{x}(t) + \widetilde{B}\hat{u}(t) = \begin{bmatrix} D_1 & & & \\ & D_2 & & \\ & & \ddots & \\ & & & D_n \end{bmatrix}\tilde{x}(t) + \frac{1}{\sqrt{n}}\begin{bmatrix} B_1 \\ B_1 \\ \vdots \\ B_1 \end{bmatrix}\hat{u}(t),$$

where $B_1 = \begin{bmatrix} 0, 1 \end{bmatrix}^{\mathsf{T}}$. Upon denoting new state variable $\tilde{x}(t)$ as $\begin{bmatrix} \tilde{x}_{11}, \tilde{x}_{12}, \tilde{x}_{21}, \tilde{x}_{22}, \ldots, \tilde{x}_{n1}, \tilde{x}_{n2} \end{bmatrix}^{\mathsf{T}}$, this system can be decoupled into n independent sub-systems $(i = 1, 2, \ldots, n)$

$$\frac{d}{dt}\begin{bmatrix} \tilde{x}_{i1} \\ \tilde{x}_{i2} \end{bmatrix} = D_i\begin{bmatrix} \tilde{x}_{i1} \\ \tilde{x}_{i2} \end{bmatrix} + \begin{bmatrix} 0 \\ \frac{1}{\sqrt{n}} \end{bmatrix}\hat{u}(t) = \begin{bmatrix} 0 & -1 + \omega^{(n-1)(i-1)} \\ \alpha_1 & -\alpha_2 + \alpha_3\omega^{(n-1)(i-1)} \end{bmatrix}\begin{bmatrix} \tilde{x}_{i1} \\ \tilde{x}_{i2} \end{bmatrix} + \begin{bmatrix} 0 \\ \frac{1}{\sqrt{n}} \end{bmatrix}\hat{u}(t).$$

We denote the controllability matrix of each sub-system as $Q_{\mathrm{c},i}$. It is easy to see that $\mathrm{rank}(Q_{\mathrm{c},1}) = 1$, indicating that the first sub-system has an uncontrollable component. Therefore, system $(\widetilde{A}, \widetilde{B})$ is not completely controllable and

has at least an uncontrollable component. In particular, the first sub-system is

$$\frac{d}{dt}\begin{bmatrix}\tilde{x}_{11}\\ \tilde{x}_{12}\end{bmatrix}=\begin{bmatrix}0 & 0\\ \alpha_1 & -\alpha_2+\alpha_3\end{bmatrix}\begin{bmatrix}\tilde{x}_{11}\\ \tilde{x}_{12}\end{bmatrix}+\begin{bmatrix}0\\ \frac{1}{\sqrt{n}}\end{bmatrix}\hat{u}(t).$$

It is clear that $\tilde{x}_{11}$ is uncontrollable and remains constant. Moreover, according to the linear transformation $\tilde{x}=(F_n^*\otimes I_2)^{-1}x$, we know that

$$\tilde{x}_{11}=\frac{1}{\sqrt{n}}\left((s_1(t)-s_{\mathrm{c}}^*)+\sum_{i=2}^{n}(s_i(t)-s^*)\right) \tag{13}$$

is constant during the dynamic evolution. In conclusion, the mixed traffic system (A,B) is not completely controllable, and has at least an uncontrollable mode (13) corresponding to a zero eigenvalue. In particular, this mode (13) corresponds to the sum of each vehicle's spacing $\sum_{i=1}^{n}s_i(t)$. As explained in the Supplementary Note 3, using the PBH test [31], we can prove that

$$\mathrm{rank}(\left[\widetilde{B},\widetilde{A}\widetilde{B},\ldots,\widetilde{A}^{2n-1}\widetilde{B}\right])=\begin{cases}2n-1, & \text{if } \alpha_1-\alpha_2\alpha_3+\alpha_3^2\neq 0,\\ n, & \text{if } \alpha_1-\alpha_2\alpha_3+\alpha_3^2=0.\end{cases}$$

Therefore, we have (6) since the controllability rank is invariant under feedback and linear transformation. Note that the condition $\alpha_1-\alpha_2\alpha_3+\alpha_3^2\neq 0$ has a probability of one when considering $\alpha_1,\alpha_2,\alpha_3$ randomly.

Predicting the final state of mixed traffic systems. For a stable system, the state will approach to its equilibrium point. In our mixed traffic system, we analyze the dynamics of each vehicle (9) and (10) separately, leading to

$$\tilde{s}_1(t_{\mathrm{f}})=s_{\mathrm{e}},\ \tilde{v}_i(t_{\mathrm{f}})=v_{\mathrm{e}},\ \tilde{s}_i(t_{\mathrm{f}})=\frac{\alpha_2-\alpha_3}{\alpha_1}v_e,\ i=2,3,\ldots,n,$$

where $s_{\mathrm{e}},v_{\mathrm{e}}$ are constant values, and t_{f} is the time when the system reaches its equilibrium point. Considering the desired state in the controller $x_{\mathrm{des}}=\left[s_c^*,v^*,s^*,v^*,\ldots,s^*,v^*\right]^{\mathsf{T}}$, the final state of the system (1) is in the form of

$$x_{\mathrm{f}}=\left[s_c^*+s_e,v^*+v_e,s^*+\frac{\alpha_2-\alpha_3}{\alpha_1}\cdot v_e,s^*+v_e,\ldots,s^*+\frac{\alpha_2-\alpha_3}{\alpha_1}\cdot v_e,v^*+v_e\right]^{\mathsf{T}}.$$

We next derive that $(s_{\mathrm{e}},v_{\mathrm{e}})$ should satisfy (7), from which we can calculate the exact value of s_e and v_e. In the final state, all the vehicles have zero acceleration, indicating that the control input $u(t)$ must be zero, *i.e.*, $u(t)=-Kx(t)=0$, leading to (7a). Besides, according to the controllability analysis, we know that $(s_1(t)-s_c^*)+\sum_{i=2}^{n}(s_i(t)-s^*)$ remains constant; see (13). Together with the system initial state and final state, we can obtain (7b).

Numerical experiments. Details of our numerical experiments and additional comparison with two heuristic control methods can be found in Supplementary Note 5. In our experiments, the standard OVM model was used to represent the human-driven car-following dynamics. All experiments were carried out in MATLAB, and the optimal control strategy was computed using the conic solver Moesk [37].

Acknowledgements

We thank A. Papachristodoulou, J. Wang, Q. Xu, L. Romao, S. Yan and C. Chen for comments and discussions. We would also like to thank R. Drummond for providing constructive feedback. Y.Z. is supported by the Clarendon Scholarship and the Jason Hu Scholarship. This work is supported by National Key R&D Program of China with 2016YFB0100906. The authors also gratefully acknowledge the support from TOYOTA.

Smoothing traffic flow via control of autonomous vehicles

Supplementary Information

Yang Zheng, Jiawei Wang, and Keqiang Li

Contents

S1. Mathematical models

In this section, we give a detailed derivation of the linearized system model shown in (1) in the main document. Two typical car-following models of human-driven vehicles, *i.e.*, the Optimal Velocity Model (OVM) [4, 30] and the Intelligent Driver Model (IDM) [3, 38], are discussed as well.

The general formulation of car-following models [3] is

$$\dot{v}_i(t) = F(s_i(t), \dot{s}_i(t), v_i(t)), \tag{S1}$$

meaning that the acceleration of a human-driven vehicle is a function of its spacing $s_i(t)$, the relative velocity between its own and its preceding vehicle $\dot{s}_i(t)$, and its velocity $v_i(t)$. Upon denoting an equilibrium state (s^*, v^*) of (S1) that satisfies

$$F(s^*, 0, v^*) = 0, \tag{S2}$$

we define the error state of the i-th human-driven vehicle as

$$\begin{cases} \tilde{s}_i(t) = s_i(t) - s^*, \\ \tilde{v}_i(t) = v_i(t) - v^*. \end{cases}$$

Then, we know that the derivative of $\tilde{s}_i(t)$ becomes

$$\dot{\tilde{s}}_i(t) = \dot{s}_i(t) = v_{i-1}(t) - v_i(t) = \tilde{v}_{i-1}(t) - \tilde{v}_i(t). \tag{S3}$$

Applying the first-order Taylor expansion to $\dot{v}_i(t) = F(s_i(t), \dot{s}_i(t), v_i(t))$ around its equilibrium point (s^*, v^*) yields

$$\begin{aligned} \dot{\tilde{v}}_i(t) = \dot{v}_i(t) &= F(s_i(t), \dot{s}_i(t), v_i(t)) - 0 \\ &= F(s_i(t), \dot{s}_i(t), v_i(t)) - F(s^*, 0, v^*) \\ &= \frac{\partial F}{\partial s}(s_i - s^*) + \frac{\partial F}{\partial \dot{s}}(\dot{s}_i - 0) + \frac{\partial F}{\partial v}(v_i - v^*) \\ &= \frac{\partial F}{\partial s}\tilde{s}_i + \frac{\partial F}{\partial \dot{s}}(\tilde{v}_{i-1} - \tilde{v}_i) + \frac{\partial F}{\partial v}\tilde{v}_i \\ &= \alpha_1 \tilde{s}_i - \alpha_2 \tilde{v}_i + \alpha_3 \tilde{v}_{i-1}, \end{aligned} \tag{S4}$$

with $\alpha_1 = \frac{\partial F}{\partial s}, \alpha_2 = \frac{\partial F}{\partial \dot{s}} - \frac{\partial F}{\partial v}, \alpha_3 = \frac{\partial F}{\partial \dot{s}}$ evaluated at the equilibrium state (s^*, v^*). These three coefficients reflect the driver's sensitivity to the error state. Considering the real driver behavior, the acceleration should increase when the spacing increases, the velocity of the ego vehicle drops, or the velocity of the preceding vehicle increases. Hence, we assume that $\alpha_1 > 0$, $\alpha_2 > 0$ and $\alpha_3 > 0$. According to (S3) and (S4), the linearized model of human-driven vehicles around the equilibrium state is

$$\begin{cases} \dot{\tilde{s}}_i = \tilde{v}_{i-1}(t) - \tilde{v}_i(t), \\ \dot{\tilde{v}}_i = \alpha_1 \tilde{s}_i(t) - \alpha_2 \tilde{v}_i(t) + \alpha_3 \tilde{v}_{i-1}(t). \end{cases} \tag{S5}$$

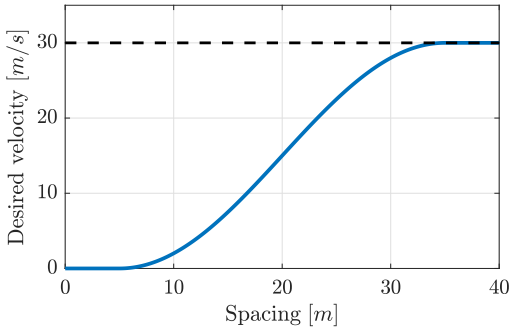

Supplementary Figure S1: Nonlinear spacing-dependent desired velocity function $V(s)$ in the OVM model. $v_{\max} = 30m/s$, $s_{\text{st}} = 5m$ and $s_{\text{go}} = 35m$. The specific mathematical expression is shown in (S7) and (S8).

In the following, we choose the OVM model and the IDM model to derive the explicit expressions of (S2) and (S5).

- The OVM model [4, 30] is given by

$$F(s_i(t), \dot{s}_i(t), v_i(t)) = \alpha(V(s_i(t)) - v_i(t)) + \beta \dot{s}_i(t), \tag{S6}$$

where $\alpha > 0$ reflects the driver's sensitivity of the difference between the current velocity and the spacing-dependent desired velocity $V(s_i(t))$, and $\beta > 0$ reflects the driver's sensitivity of the difference between the velocities of the ego vehicle and the preceding vehicle. $V(s_i(t))$ is usually modeled by a continuous piecewise function

$$V(s) = \begin{cases} 0, & s \leq s_{\text{st}}, \\ f_v(s), & s_{\text{st}} < s < s_{\text{go}}, \\ v_{\max}, & s \geq s_{\text{go}}, \end{cases} \tag{S7}$$

where the desired velocity $V(s)$ is zero for small spacing s_{st}, and reach a maximum value $v_{\max}$ for large spacing s_{go}, and $f_v(s)$ is a monotonically increasing function and defines the desired velocity when the spacing s is between s_{st} and s_{go}. There are many choices of $f_v(s)$, either in a linear or nonlinear form. A typical one is the following nonlinear form,

$$f_v(s) = \frac{v_{\max}}{2}\left(1 - \cos(\pi \frac{s - s_{\text{st}}}{s_{\text{go}} - s_{\text{st}}})\right). \tag{S8}$$

A typical example of $V(s)$ is shown in Figure S1. For the general OVM model (S6), it is easy to obtain the following specific equilibrium state (s^*, v^*) that satisfies (S2)

$$v^* = V(s^*). \tag{S9}$$

Furthermore, we can calculate the values of the coefficients in linearized model (S5) as follows

$$\alpha_1 = \alpha \dot{V}(s^*),\ \alpha_2 = \alpha + \beta,\ \alpha_3 = \beta, \tag{S10}$$

where $\dot{V}(s^*)$ denotes the derivative of $V(s)$ with respect to s evaluated at the equilibrium spacing s^*.

- The IDM model [3, 38] is defined as

$$F(s_i(t), \dot{s}_i(t), v_i(t)) = a\left(1 - \left(\frac{v}{v_{\max}}\right)^4 - \left(\frac{s_{\text{st}} + T_{\text{gap}} v - \frac{\dot{s}v}{\sqrt{4ab}}}{s}\right)^2\right),$$

where a and b are the maximum acceleration and the comfortable deceleration respectively, and T_{gap} is the desired time headway for the driver. Using (S2), we can obtain the equilibrium state equation for IDM as

$$s^* = \frac{s_{\text{st}} + T_{\text{gap}} v^*}{\sqrt{1 - (\frac{v^*}{v_{\max}})^4}}. \tag{S11}$$

Moreover, the coefficients of the linearized model (S5) in the case of IDM are

$$\begin{aligned}
\alpha_1 &= 2a \cdot \frac{(s_{\text{st}} + T_{\text{gap}} v^*)^2}{(s^*)^3}, \\
\alpha_2 &= \sqrt{\frac{a}{b}} \cdot \frac{v^* (s_{\text{st}} + T_{\text{gap}} v^*)}{(s^*)^2} + 2a\left(\frac{2(v^*)^3}{v_{\max}^4} + \frac{T_{\text{gap}}(s_{\text{st}} + T_{\text{gap}} v^*)}{(s^*)^2}\right), \\
\alpha_3 &= \sqrt{\frac{a}{b}} \cdot \frac{v^* (s_{\text{st}} + T_{\text{gap}} v^*)}{(s^*)^2}.
\end{aligned}$$

In the rest of this section, we derive the model for the mixed traffic system with one autonomous vehicle. For the autonomous vehicle, we use the acceleration signal as the control input, *i.e.*, $\dot{v}_i(t) = u_i(t)$. Then, the car-following model of the autonomous vehicle is

$$\begin{cases}
\dot{\tilde{s}}_1 = \tilde{v}_n(t) - \tilde{v}_1(t), \\
\dot{\tilde{v}}_1 = u(t).
\end{cases}$$

Upon combining the error states of all the vehicles as the mixed traffic system state, $x(t) = \left[x_1^{\mathsf{T}}(t), x_2^{\mathsf{T}}(t), \ldots, x_n^{\mathsf{T}}(t)\right]^{\mathsf{T}}$, where $x_1(t) = \left[s_1(t) - s_{\text{c}}^*, v_1(t) - v^*\right]^{\mathsf{T}}$ and $x_i(t) = \left[s_i(t) - s^*, v_i(t) - v^*\right]^{\mathsf{T}}, i = 2, \ldots, n$, we obtain the linearized dynamics of the mixed traffic system with one autonomous vehicle as follows

$$\dot{x}(t) = Ax(t) + Bu(t) = \begin{bmatrix}
C_1 & 0 & \ldots & \ldots & 0 & C_2 \\
A_2 & A_1 & 0 & \ldots & \ldots & 0 \\
0 & A_2 & A_1 & 0 & \ldots & 0 \\
\vdots & \ddots & \ddots & \ddots & \ddots & \vdots \\
0 & \ldots & 0 & A_2 & A_1 & 0 \\
0 & \ldots & \ldots & 0 & A_2 & A_1
\end{bmatrix} x(t) + \begin{bmatrix}
B_1 \\ B_2 \\ B_2 \\ \vdots \\ B_2
\end{bmatrix} u(t), \tag{S12}$$

where each block matrix is given by

$$A_1 = \begin{bmatrix} 0 & -1 \\ \alpha_1 & -\alpha_2 \end{bmatrix}, A_2 = \begin{bmatrix} 0 & 1 \\ 0 & \alpha_3 \end{bmatrix}, C_1 = \begin{bmatrix} 0 & -1 \\ 0 & 0 \end{bmatrix}, C_2 = \begin{bmatrix} 0 & 1 \\ 0 & 0 \end{bmatrix}, B_1 = \begin{bmatrix} 0 \\ 1 \end{bmatrix}, B_2 = \begin{bmatrix} 0 \\ 0 \end{bmatrix}. \tag{S13}$$

S2. Analytical stability results

In equation (11) of the main document, we have defined $H(\lambda)$ as

$$H(\lambda) = \frac{\alpha_1 + \alpha_3\lambda}{\alpha_1 + \alpha_2\lambda + \lambda^2},$$

leading to the following equation

$$H(\lambda) = e^{\frac{i-1}{n}\cdot 2\pi j}, \quad i = 1, 2, \ldots, n. \tag{S14}$$

The rest of analysis follows [18] to derive the stability result (5) in the main text. In particular, it is easy to see that the eigenvalues of $\hat{A}$ correspond to the solutions of (S14). Note that $e^{\frac{i-1}{n}\cdot 2\pi j}$ is the i-th complex root of $z^n = 1$, indicating that for all the eigenvalues λ of A, the values of $H(\lambda)$ constitute n unit roots. As n changes, $H(\lambda)$ corresponds to different unit roots. Therefore, if all the roots of $|H(\lambda)| = 1$ have negative real parts, then the solutions of equation (S14), *i.e.*, the eigenvalues of matrix $\hat{A}$, have negative real parts. We conclude that the condition that all the roots of $|H(\lambda)| = 1$ have negative real parts is sufficient to guarantee that $\hat{A}$ is stable. Note that this condition becomes sufficient and necessary for the case where the system is stable for any n. This is because that $H(\lambda)$ can be any unit root $e^{\theta j}$, for $\theta \in [0, 2\pi)$.

Since all rational functions are meromorphic, $H(\lambda)$ is a meromorphic function. Because α_1 and α_2 are positive real numbers, the poles of $H(\lambda)$ are in the left half plane, indicating that $H(\lambda)$ is holomorphic in the right half plane. Meanwhile, $|H(\lambda)| \to 0$ when $\mathrm{Re}(\lambda) \to \infty$. According to Maximum Modulus Principle [39], the extreme value of $|H(\lambda)|$ in the right half plane can only be obtained on the imaginary axis. To avoid eigenvalues with positive real parts, $|H(\lambda)|$ should not be more than 1 on the imaginary axis. Therefore, that the roots of $|H(\lambda)| = 1$ have negative real part is equivalent to $|H(jv)| \leq 1, \ \forall v \in \mathbb{R}$. This inequality leads to the stability criterion

$$\alpha_2^2 - \alpha_3^2 - 2\alpha_1 \geq 0. \tag{S15}$$

Substituting (S10) into (S15), the stability criterion for the OVM model is

$$\alpha + 2\beta \geq \dot{V}(s^*).$$

Remark 1 (Marginal Stability)**.** *From equation (10) of the main document or* (S14)*, when $i = 1$, we have $\lambda^2 + (\alpha_2 - \alpha_3)\lambda = 0$. This indicates we always have $\lambda = 0$, which is independent of α_1, α_2 and α_3. It means that there always exists a zero eigenvalue for $\hat{A}$. Therefore, the system is marginally stable, and indeed, the zero eigenvalue corresponds to the ring structure of the system. We shall show that this feature of zero eigenvalue is inherent even when we introduce an autonomous vehicle into the traffic system.*

S3. Controllability analysis

We use a block circulant matrix diagonalization method to analyze the controllability of system (A, B) shown in (S12), and prove that the rank of the controllability matrix Q_{c} is either $2n-1$ or n; see (6) in the main text. Before continuing our analysis, we present four useful lemmas on the controllability of linear systems [31, 40].

Lemma 1 (Controllability)**.** *The linear system (A, B) is controllable if and only if rank $\left[B, AB, \ldots, A^{2n-1}B\right] = 2n$.*

Lemma 1 is the well-known Kalman's controllability rank test [40], which provides a necessary and sufficient mathematical condition for controllability. However, computing the rank requires all the elements of (A, B) to be known, and it might be not numerically reliable to calculate the rank for large-scale systems. To facilitate analytical analysis, it may be desirable to apply a certain *linear transformation*, thus representing the linear system under a different basis and simplifying the system dynamics.

In particular, given a nonsingular T, we define a new state $\tilde{x} = T^{-1}x$, leading to the following dynamics

$$\dot{\tilde{x}}(t) = T^{-1}AT\tilde{x}(t) + T^{-1}Bu(t).$$

Then, we obtain an equivalent linear system $(T^{-1}AT, T^{-1}B)$, which should have the same controllability as that of (A, B). This conclusion is formally presented in Lemma 2.

Lemma 2 (Invariance under linear transformation)**.** *The linear system (A, B) is controllable if and only if $(T^{-1}AT, T^{-1}B)$ is controllable for every nonsingular T.*

If one can diagonalize the system matrix A via $T^{-1}AT$, then the controllability of (A, B) will be easier to derive by checking the controllability of $(T^{-1}AT, T^{-1}B)$. Sometimes, this diagonalization may be nontrivial for its original form (A, B). In this case, it may be desirable to apply certain state feedback to simply the system dynamics before looking for diagonalization. Specifically, consider a control law $v(t) = u(t) + Kx(t)$, and we arrive at

$$\dot{x}(t) = (A - BK)x(t) + Bv(t),$$

This linear system $(A - BK, B)$ also have the same controllability with (A, B), which is formally summarized in the following lemma.

Lemma 3 (Invariance under state feedback)**.** *The linear system (A, B) is controllable if and only if $(A - BK, B)$ is controllable for every K with compatible dimension.*

In addition, we will rely on the following PBH test for our controllability analysis.

Lemma 4 (PBH controllability criterion)**.** *The linear system (A, B) is controllable if and only if rank$(\lambda I - A, B) = 2n$ for every eigenvalue λ of A. In addition, (A, B) is uncontrollable if and only if there exists $\omega \neq 0$, such that*

$$\omega^{\mathsf{T}}A = \lambda\omega^{\mathsf{T}}, \omega^{\mathsf{T}}B = 0,$$

where ω is a left eigenvector of A corresponding to λ, and ω corresponds to an uncontrollable mode.

Now, we are ready to show that the mixed traffic system (S12) is not completely controllable. Our main idea is to exploit the invariance of controllability under linear transformation and state feedback. Using a sequence of state feedback and linear transformation, we diagonalize the system (A, B), leading to an analytical conclusion on the controllability of (S12). Our procedure is as follows.

$$(A, B) \quad \xrightarrow{\text{state feedback}} \quad (\hat{A}, B) \quad \xrightarrow{\text{linear transformation}} \quad (\widetilde{A}, \widetilde{B})$$

First, we transform system (A, B) into $(\hat{A}, B)$ by introducing a virtual input $\hat{u}(t)$, defined as $\hat{u}(t) = u(t) - (\alpha_1 \tilde{s}_1(t) - \alpha_2 \tilde{v}_1(t) + \alpha_3 \tilde{v}_n(t))$, which is the difference between the actual control value and the acceleration value when the vehicle is controlled by a human driver. Then, the state space model of $(\hat{A}, B)$ becomes

$$\dot{x}(t) = \hat{A}x(t) + B\hat{u}(t) = \begin{bmatrix} A_1 & 0 & \dots & \dots & 0 & A_2 \\ A_2 & A_1 & 0 & \dots & \dots & 0 \\ 0 & A_2 & A_1 & 0 & \dots & 0 \\ \vdots & \ddots & \ddots & \ddots & \ddots & \vdots \\ 0 & \dots & 0 & A_2 & A_1 & 0 \\ 0 & \dots & \dots & 0 & A_2 & A_1 \end{bmatrix} x(t) + \begin{bmatrix} B_1 \\ B_2 \\ B_2 \\ \vdots \\ B_2 \end{bmatrix} \hat{u}(t).$$

The controllability remains the same between system $(\hat{A}, B)$ and the original system (A, B). Now, note that $\hat{A}$ is block circulant, and we can use the block diagonalization method [28, 29] to analyze the controllability of $(\hat{A}, B)$. Precisely, we use the transformation matrix $F_n^* \otimes I_2$ to transform $(\hat{A}, B)$ into $(\widetilde{A}, \widetilde{B})$, and the new system matrix is

$$\widetilde{A} = (F_n^* \otimes I_2)^{-1} \hat{A} (F_n^* \otimes I_2) = \operatorname{diag}(D_1, D_2, \dots, D_n). \tag{S16}$$

The new state variable $\tilde{x}$ after transformation becomes

$$\tilde{x} = (F_n^* \otimes I_2)^{-1} x = (F_n \otimes I_2) x, \tag{S17}$$

and the new control matrix $\widetilde{B}$ is

$$\widetilde{B} = (F_n^* \otimes I_2)^{-1} B = (F_n \otimes I_2) B = \frac{1}{\sqrt{n}} \begin{bmatrix} I_2 & I_2 & I_2 & \cdots & I_2 \\ I_2 & \bar{\omega} I_2 & \bar{\omega}^2 I_2 & \cdots & \bar{\omega}^{n-1} I_2 \\ I_2 & \bar{\omega}^2 I_2 & \bar{\omega}^4 I_2 & \cdots & \bar{\omega}^{2(n-1)} I_2 \\ \vdots & \vdots & \vdots & & \vdots \\ I_2 & \bar{\omega}^{n-1} I_2 & \bar{\omega}^{2(n-1)} I_2 & \cdots & \bar{\omega}^{(n-1)(n-1)} I_2 \end{bmatrix} \begin{bmatrix} B_1 \\ B_2 \\ \vdots \\ B_2 \end{bmatrix} = \frac{1}{\sqrt{n}} \begin{bmatrix} B_1 \\ B_1 \\ \vdots \\ B_1 \end{bmatrix},$$

where $\bar{\omega}$ is the conjugate transpose of ω. Therefore, the dynamics of $\tilde{x}$ are

$$\dot{\tilde{x}} = \widetilde{A}\tilde{x}(t) + \widetilde{B}\hat{u}(t) = \begin{bmatrix} D_1 & & & \\ & D_2 & & \\ & & \ddots & \\ & & & D_n \end{bmatrix} \tilde{x}(t) + \frac{1}{\sqrt{n}} \begin{bmatrix} B_1 \\ B_1 \\ \vdots \\ B_1 \end{bmatrix} \hat{u}(t). \tag{S18}$$

Upon denoting $\tilde{x}(t) = \left[\tilde{x}_{11}, \tilde{x}_{12}, \tilde{x}_{21}, \tilde{x}_{22}, \ldots, \tilde{x}_{n1}, \tilde{x}_{n2}\right]^{\mathsf{T}}$, $(\widetilde{A}, \widetilde{B})$ is decoupled into n independent subsystems

$$\frac{d}{dt}\begin{bmatrix} \tilde{x}_{i1} \\ \tilde{x}_{i2} \end{bmatrix} = D_i \begin{bmatrix} \tilde{x}_{i1} \\ \tilde{x}_{i2} \end{bmatrix} + \begin{bmatrix} 0 \\ \frac{1}{\sqrt{n}} \end{bmatrix} \hat{u}(t) = \begin{bmatrix} 0 & -1 + \omega^{(n-1)(i-1)} \\ \alpha_1 & -\alpha_2 + \alpha_3\omega^{(n-1)(i-1)} \end{bmatrix} \begin{bmatrix} \tilde{x}_{i1} \\ \tilde{x}_{i2} \end{bmatrix} + \begin{bmatrix} 0 \\ \frac{1}{\sqrt{n}} \end{bmatrix} \hat{u}(t).$$

The rank of the controllability matrix $Q_{\mathrm{c},i}$ of each sub-system is

$$\operatorname{rank}(Q_{\mathrm{c},i}) = \operatorname{rank}\left(\begin{bmatrix} 0 & \left(-1 + \omega^{(n-1)(i-1)}\right)\frac{1}{\sqrt{n}} \\ \frac{1}{\sqrt{n}} & \left(-\alpha_2 + \alpha_3\omega^{(n-1)(i-1)}\right)\frac{1}{\sqrt{n}} \end{bmatrix} \right).$$

It is not difficult to see $\operatorname{rank}(Q_{\mathrm{c},1}) = 1$, meaning that the first sub-system has an uncontrollable component. Therefore, the system pair $(\widetilde{A}, \widetilde{B})$ is not completely controllable and has at least an uncontrollable component. In particular, the uncontrollable sub-system is

$$\frac{d}{dt}\begin{bmatrix} \tilde{x}_{11} \\ \tilde{x}_{12} \end{bmatrix} = \begin{bmatrix} 0 & 0 \\ \alpha_1 & -\alpha_2 + \alpha_3 \end{bmatrix} \begin{bmatrix} \tilde{x}_{11} \\ \tilde{x}_{12} \end{bmatrix} + \begin{bmatrix} 0 \\ \frac{1}{\sqrt{n}} \end{bmatrix} \hat{u}(t),$$

meaning that $\tilde{x}_{11}$ is an uncontrollable component, and $\tilde{x}_{11}$ remains constant during the dynamic evolution. According to $\widetilde{x} = (F_n^* \otimes I_2)^{-1}x$, we know that

$$\tilde{x}_{11} = \frac{1}{\sqrt{n}}\left((s_1(t) - s_c^*) + \sum_{i=2}^{n} (s_i(t) - s^*) \right) \tag{S19}$$

is uncontrollable and remains constant. This exactly corresponds to the ring structure. Note that system $(\tilde{A}, \tilde{B})$ is equivalent to system $(\hat{A}, B)$ due to the linear transformation. Also, system $(\hat{A}, B)$ has the same controllability characteristic as the original system (A, B). Therefore, we conclude that the original system pair (A, B) is not completely controllable and has at least one uncontrollable component which remains constant, as shown in (S19).

After revealing the uncontrollable component (S19), we next use Lemma 4 to prove

$$\operatorname{rank}(Q_c) = \operatorname{rank}\left(\left[\widetilde{B}, \widetilde{A}\widetilde{B}, \ldots, \widetilde{A}^{2n-1}\widetilde{B}\right] \right) = \begin{cases} 2n-1, & \text{if } \alpha_1 - \alpha_2\alpha_3 + \alpha_3^2 \neq 0, \\ n, & \text{if } \alpha_1 - \alpha_2\alpha_3 + \alpha_3^2 = 0. \end{cases}$$

- Case 1: $\alpha_1 - \alpha_2\alpha_3 + \alpha_3^2 \neq 0$. For convenience, we restate the eigenvalue calculation (11) as

$$\begin{aligned}\det(\lambda I - \widetilde{A}) &= \prod_{i=1}^{n} \det(\lambda I - D_i) \\ &= \prod_{i=1}^{n} \left(\lambda^2 + \left(\alpha_2 - \alpha_3\omega^{(n-1)(i-1)}\right)\lambda + \alpha_1\left(1 - \omega^{(n-1)(i-1)}\right)\right) \\ &= 0.\end{aligned}$$

where each block D_i is

$$D_i = \begin{bmatrix} 0 & -1 + \omega^{(n-1)(i-1)} \\ \alpha_1 & -\alpha_2 + \alpha_3\omega^{(n-1)(i-1)} \end{bmatrix},\ i = 1, 2, \ldots, n. \tag{S20}$$

Step 1: We first prove that D_i and D_j $(i \neq j)$ share no common eigenvalues. Assume there exists a λ satisfying $\det(\lambda I - D_i) = 0$ and $\det(\lambda I - D_j) = 0$, $i \neq j$, which means

$$\begin{cases} \lambda^2 + \alpha_2\lambda + \alpha_1 = (\alpha_3\lambda + \alpha_1)\omega^{(n-1)(i-1)}, \\ \lambda^2 + \alpha_2\lambda + \alpha_1 = (\alpha_3\lambda + \alpha_1)\omega^{(n-1)(j-1)}. \end{cases}$$

Since $\omega^{(n-1)(i-1)} \neq \omega^{(n-1)(j-1)}$, we obtain $\alpha_3\lambda + \alpha_1 = 0$ and $\lambda^2 + \alpha_2\lambda + \alpha_1 = 0$, leading to

$$\alpha_1 - \alpha_2\alpha_3 + \alpha_3^2 = 0,\ \lambda = \alpha_3 - \alpha_2,$$

which contradicts the condition that $\alpha_1 - \alpha_2\alpha_3 + \alpha_3^2 \neq 0$. Therefore, D_i and $D_j, j \neq i$ have different eigenvalues.

Step 2: We then prove that all the system modes corresponding to non-zero eigenvalues are controllable. Denote $\lambda_k \neq 0$ as the eigenvalue of D_k and ρ as its corresponding left eigenvector. According to Lemma 4, we need to show $\rho^{\mathsf{T}}\widetilde{B} \neq 0$.

Upon denoting ρ as $\rho = \left[\rho_1^{\mathsf{T}}, \rho_2^{\mathsf{T}}, \ldots, \rho_n^{\mathsf{T}}\right]^{\mathsf{T}}$ where $\rho_i = \left[\rho_{i1}, \rho_{i2}\right]^{\mathsf{T}} \in \mathbb{R}^{2\times 1}, i = 1, 2, \ldots, n$, the condition $\rho^{\mathsf{T}}\widetilde{A} = \lambda_k\rho^{\mathsf{T}}$ leads to

$$\rho_i^{\mathsf{T}} D_i = \lambda_k \rho_i^{\mathsf{T}},\ i = 1, 2, \ldots, n. \tag{S21}$$

Because λ_k is not an eigenvalue of D_i, $i \neq k$, we obtain $\rho_i = 0$, $i \neq k$. Hence, $\rho^{\mathsf{T}}\widetilde{B} = \rho_k^{\mathsf{T}} B_1 = \rho_{k2}$. Assume $\rho_{k2} = 0$, and then substituting (S20) into (S21) yields

$$\begin{bmatrix} \rho_{k1} & 0 \end{bmatrix} \begin{bmatrix} 0 & -1 + \omega^{(n-1)(k-1)} \\ \alpha_1 & -\alpha_2 + \alpha_3\omega^{(n-1)(k-1)} \end{bmatrix} = \lambda_k \begin{bmatrix} \rho_{k1} & 0 \end{bmatrix}. \tag{S22}$$

The only solution to (S22) is $\rho_{k1} = 0$, indicating that the left eigenvector $\rho = 0$, which is false. Accordingly, the assumption that $\rho_{k2} = 0$ does not hold. Therefore, we have $\rho^{\mathsf{T}}\widetilde{B} = \rho_{k2} \neq 0$, meaning that the mode corresponding to λ_k is controllable. In other words, the system modes corresponding to nonzero eigenvalues

are all controllable. Because the only zero eigenvalue $\lambda = 0$ appears in $\det(\lambda I - D_1) = 0$, and we have shown in equation (S19) that the corresponding mode is uncontrollable. Consequently, we conclude that if $\alpha_1 - \alpha_2\alpha_3 + \alpha_3^2 \neq 0$, there are $2n-1$ controllable modes in the system $(\widetilde{A}, \widetilde{B})$, meaning that $\text{rank}(Q_c) = 2n-1$.

- Case 2: $\alpha_1 - \alpha_2\alpha_3 + \alpha_3^2 = 0$. Substituting this condition into $\det(\lambda I - D_i) = 0$ yields

$$\begin{aligned}\det(\lambda I - D_i) &= \lambda^2 + \left(\alpha_2 - \alpha_3\omega^{(n-1)(i-1)}\right)\lambda + \alpha_1\left(1 - \omega^{(n-1)(i-1)}\right)\\ &= (\lambda + \alpha_2 - \alpha_3)\left(\lambda + \alpha_3 - \alpha_3\omega^{(n-1)(i-1)}\right)\\ &= 0,\ i = 1, 2, \ldots, n,\end{aligned}$$

which gives the eigenvalues of $D_i,\ i = 1, 2, \ldots, n$ as follows

$$\lambda_{i1} = \alpha_3 - \alpha_2,\ , \lambda_{i2} = \alpha_3\left(\omega^{(n-1)(i-1)} - 1\right).$$

Step 1: we prove that there are $n-1$ uncontrollable modes corresponding to $\alpha_3 - \alpha_2$. It is easy to see that $\alpha_3 - \alpha_2$ is the common eigenvalue for each block $D_i,\ i = 1, 2, \ldots, n$, *i.e.*, the algebraic multiplicity of $\alpha_3 - \alpha_2$ is n. We consider its left eigenvector $\rho = \left[\rho_1^\mathsf{T}, \rho_2^\mathsf{T}, \ldots, \rho_n^\mathsf{T}\right]^\mathsf{T}$. Similar to (S21), we obtain

$$\rho_i^\mathsf{T} D_i = (\alpha_3 - \alpha_2)\rho_i^\mathsf{T},\ i = 1, 2, \ldots, n.$$

Expanding this equation leads to

$$\begin{bmatrix}\rho_{i1} & \rho_{i2}\end{bmatrix}\begin{bmatrix}0 & -1 + \omega^{(n-1)(i-1)}\\ \alpha_1 & -\alpha_2 + \alpha_3\omega^{(n-1)(i-1)}\end{bmatrix} = (\alpha_3 - \alpha_2)\begin{bmatrix}\rho_{i1} & \rho_{i2}\end{bmatrix},\ i = 1, 2, \ldots, n,$$

from which we have $\rho_{i1} = -\alpha_3\rho_{i2},\ i = 1, 2, \ldots, n$. Therefore, we can choose n linearly independent left eigenvectors corresponding to $\alpha_3 - \alpha_2$ as

$$\begin{aligned}\rho^{(1)} &= \left[-\alpha_3, 1, 0, 0, 0, 0, \ldots, 0, 0\right],\\ \rho^{(2)} &= \left[-\alpha_3, 1, \alpha_3, -1, 0, 0, \ldots, 0, 0\right],\\ \rho^{(3)} &= \left[-\alpha_3, 1, 0, 0, \alpha_3, -1, \ldots, 0, 0\right],\\ &\vdots\\ \rho^{(n)} &= \left[-\alpha_3, 1, 0, 0, 0, 0 \ldots, \alpha_3, -1\right].\end{aligned} \tag{S23}$$

From these left eigenvectors, it is easy to verify that $\left(\rho^{(1)}\right)^\mathsf{T}\widetilde{B} \neq 0$ and $\left(\rho^{(i)}\right)^\mathsf{T}\widetilde{B} = 0,\ i = 2, 3, \ldots, n$, meaning that for $\alpha_3 - \alpha_2$, there are $n-1$ uncontrollable modes.

Step 2: we consider the rest of eigenvalues, *i.e.* $\lambda_{i2} = \alpha_3\left(\omega^{(n-1)(i-1)} - 1\right),\ i = 1, 2, \ldots, n$. The zero eigenvalue $\lambda_{12} = 0$ still corresponds to an uncontrollable mode, as shown in (S19). We prove that the modes associated with $\lambda_{i2} = \alpha_3\left(\omega^{(n-1)(i-1)} - 1\right),\ i = 2, 3, \ldots, n$ are controllable. The proof is similar to the scenario where we have

$\alpha_1-\alpha_2\alpha_3+\alpha_3^2\neq 0$. For $\lambda_{k2}=\alpha_3\left(\omega^{(n-1)(k-1)}-1\right),\ (k\neq 1)$, denote its left eigenvector as $\rho=\left[\rho_1^{\mathsf{T}},\rho_2^{\mathsf{T}},\ldots,\rho_n^{\mathsf{T}}\right]^{\mathsf{T}}$, where $\rho_i=\left[\rho_{i1},\rho_{i2}\right]^{\mathsf{T}}\in\mathbb{R}^{2\times 1}, i=1,2,\ldots,n$. Then we have $\rho_i=0,\ i\neq k$, since λ_{k2} is not an eigenvalue of other blocks $D_i,\ i\neq k$. For $\rho_k=\left[\rho_{k1},\rho_{k2}\right]^{\mathsf{T}}$, we have $\rho_{k2}\neq 0$, which is similar to the argument in (S22). Therefore, $\rho^{\mathsf{T}}\widetilde{B}\neq 0$, meaning the mode corresponding to $\lambda_{k2}, k\neq 1$ is controllable.

In summary, the eigenvalue $\lambda=\alpha_3-\alpha_2$ is associated with $n-1$ uncontrollable modes and 1 controllable mode. Since $\alpha_3-\alpha_2<0$, the uncontrollable modes are all stable. In addition, the $n-1$ modes associated with $\lambda_{i2}=\alpha_3\left(\omega^{(n-1)(i-1)}-1\right),\ i=2,3,\ldots,n$ are controllable, and the zero eigenvalue corresponds to an uncontrollable mode. In total, there are n controllable modes in the system $(\widetilde{A},\widetilde{B})$, meaning that $\mathrm{rank}(Q_c)=n$.

Remark 2 (Stabilizability of mixed traffic systems)**.** *In the mixed traffic system with one autonomous vehicle,* i.e.*, the system pair (A,B), the uncontrollable mode corresponds to a zero eigenvalue, and the rest of modes are either controllable or stable. Therefore, system (A,B) is stabilizable. In particular, by choosing an appropriate control input, the autonomous vehicle can not only stabilize the global traffic flow, but also steer the system to a higher equilibrium traffic speed; see Figure 4 in the main text for illustration.*

S4. Solution method for the optimal control strategy

We have shown that a mixed traffic system with a single autonomous vehicle is stabilizable. Following the standard control theory [31], we design an optimal control strategy to reject perturbations in the mixed traffic system. In our framework, we model this scenario by assuming that there exists a disturbance signal $w_i(t)$ in each vehicle's acceleration signal, *i.e.*, $\dot{\tilde{v}}_i=\alpha_1\tilde{s}_i(t)-\alpha_2\tilde{v}_i(t)+\alpha_3\tilde{v}_{i-1}(t)+w_i(t)$. In other words, the linearized dynamics of human-driven vehicle (S5) become

$$\dot{x}_i(t)=A_1x_i(t)+A_2x_{i-1}(t)+H_1w_i(t),$$

where $H_1=\left[0,1\right]^{\mathsf{T}}$. Then, we design an optimal control input $u(t)=-Kx(t)$ to minimize the influence of disturbances $w_i(t)$ on the traffic system, where $K\in\mathbb{R}^{1\times 2n}$ denotes the feedback gain. Mathematically, this can be formulated into the following optimization problem

$$\begin{aligned}\min_{K}\quad & \|G_{wz}\|\\ \text{subject to}\quad & u=-Kx,\end{aligned}\tag{S24}$$

where G_{wz} denotes the transfer function from disturbance signal $w(t)=\left[w_1(t),\ldots,w_n(t)\right]$ to the traffic performance state $z(t)=\left[\gamma_s\tilde{s}_1(t),\gamma_v\tilde{v}_1(t),\ldots,\gamma_s\tilde{s}_n(t),\gamma_v\tilde{v}_n(t),\gamma_u u(t)\right]^{\mathsf{T}}$, with positive weights $\gamma_s>0,\gamma_v>0,\gamma_u>0$, and $\|\cdot\|$ denotes the $\mathcal{H}_2$ norm of a transfer function that captures the influence of disturbances. Note that the performance state can also be written into

$$z(t)=\begin{bmatrix}Q^{\frac{1}{2}}\\ 0\end{bmatrix}x(t)+\begin{bmatrix}0\\ R^{\frac{1}{2}}\end{bmatrix}u(t),$$

where $Q^{\frac{1}{2}} = \text{diag}(\gamma_s, \gamma_v, \ldots, \gamma_s, \gamma_v)$ and $R^{\frac{1}{2}} = \gamma_u$ denote the square roots of state and control performance weights, respectively.

Solution via convex optimization. The optimization problem (S24) is in the standard form of the $\mathcal{H}_2$ optimal controller synthesis in control theory [31]. Here, we briefly present the steps to obtain a convex formulation for problem (S24). It is known that the $\mathcal{H}_2$ norm of a stable linear system can be calculated as follows.

Lemma 5 ([31]). *Given a stable linear system $\dot{x}(t) = Ax(t) + Hw(t), z(t) = Cx(t)$, the $\mathcal{H}_2$ norm of the transfer function from disturbance $w(t)$ to performance signal $z(t)$ can be computed by*

$$\|G_{wz}\|^2 = \inf_{X \succ 0} \{ \mathit{Trace}\big(CXC^\mathsf{T}\big) \mid AX + XA^\mathsf{T} + HH^\mathsf{T} \preceq 0 \}.$$

where $\mathit{Trace}(\cdot)$ denotes the trace of a symmetric matrix.

When applying state-feedback $u = -Kx$, the closed-loop traffic system becomes

$$\begin{aligned} \dot{x}(t) &= (A - BK)x(t) + Hw(t), \\ z(t) &= \begin{bmatrix} Q^{\frac{1}{2}} \\ -R^{\frac{1}{2}}K \end{bmatrix} x(t). \end{aligned}$$

Using Lemma 5 and a standard change of variables $Z = KX$, the optimal control problem (S24) can be equivalently reformulated as

$$\begin{aligned} \min_{X,Z} \quad & \text{Trace}(QX) + \text{Trace}\left(RZX^{-1}Z^\mathsf{T}\right) \\ \text{subject to} \quad & (AX - BZ) + (AX - BZ)^\mathsf{T} + HH^\mathsf{T} \preceq 0, \\ & X \succ 0. \end{aligned}$$

By introducing $Y \succeq ZX^{-1}Z^\mathsf{T}$ and using the Schur complement, a convex reformulation to (S24) is derived as follows.

$$\begin{aligned} \min_{X,Y,Z} \quad & \text{Trace}(QX) + \text{Trace}(RY) \\ \text{subject to} \quad & (AX - BZ) + (AX - BZ)^\mathsf{T} + HH^\mathsf{T} \preceq 0, \\ & \begin{bmatrix} Y & Z \\ Z^\mathsf{T} & X \end{bmatrix} \succeq 0, X \succ 0. \end{aligned} \tag{S25}$$

Problem (S25) is convex and ready to be solved using general solvers, *e.g.*, Mosek [37], and the optimal controller is recovered as $K = ZX^{-1}$.

Implementation of the optimal control strategy. Upon choosing the weight coefficients γ_s, γ_v, and γ_u, we can solve (S25) to obtain an optimal control strategy $u(t) = -Kx(t)$ to reject the influence of disturbances. Considering

the definition of state $x(t)$ and denoting $K = \left[k_{1,1}, k_{1,2}, k_{2,1}, k_{2,2,}, \ldots, k_{n,1}, k_{n,2}\right] \in \mathbb{R}^{1\times 2n}$, the optimal control strategy is implemented as

$$u(t) = -\left(k_{1,1}\left(s_1(t) - s_c^*\right) + k_{1,2}\left(v_1(t) - v^*\right) + \sum_{i=2}^{n}\left(k_{i,1}(s_i(t) - s^*) + k_{i,2}(v_i(t) - v^*)\right)\right), \tag{S26}$$

where (s^*, v^*) is the traffic equilibrium state of human-driven vehicles satisfying (S2), and $s_c^* > 0$ is the desired spacing for the autonomous vehicle that is free to choose. For the OVM model, (s^*, v^*) should satisfy (S9), while for the IDM model, (s^*, v^*) should meet (S11).

As discussed in the section of *reachability and system final state* in the main document, by choosing the equilibrium state (s^*, v^*) and s_c^* properly in (S26), we can not only stabilize the global traffic flow but also steer the traffic flow to a higher traffic velocity v^*; see Figure 4 in the main document for numerical illustration. Note that the maximum reachable traffic velocity v^* is determined by its corresponding maximum reachable spacing s^*, as shown in equation 8. Figure S2 illustrates the scenario where the autonomous vehicle increase the equilibrium traffic speed.

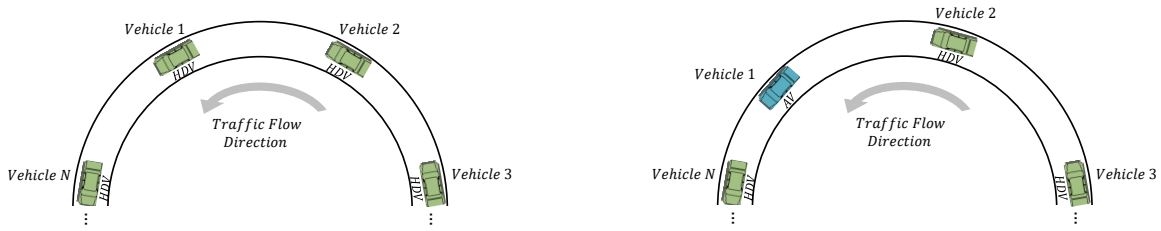

Supplementary Figure S2: Illustration of the scenario where the autonomous vehicle increases the traffic speed, AV: autonomous vehicle; HDV: human-driven vehicle. (a) When all vehicles are human-driven, the spacing between two vehicles is equal for homogeneous car-following dynamics. (b) In the case of mixed traffic systems, the autonomous vehicle be controlled to follow its preceding vehicle in a shorter distance, and the other human-driven vehicles have a larger spacing at the equilibrium state. According to $F(s^*, 0, v^*) = 0$, the equilibrium velocity v^* increases as s^* grows up. Hence, the entire traffic flow speed can be increased via controlling the autonomous vehicle; see Figure 4(b) for a numerical demonstration.

S5. Additional numerical experiments: numerical comparison

In this section, we compare our proposed method in the mixed traffic system with only one AV, with two existing controllers, FollowerStopper and PI with Saturation [19]. We conducted two types of simulations representing different traffic situations, and we used the nonlinear OVM model (S6)—(S8) for human-driven vehicles. Throughout our numerical experiments, the parameters for the OVM model were $\alpha = 0.6$, $\beta = 0.9$, $v_{\max} = 30m/s$, $s_{\text{st}} = 5m$, and $s_{\text{go}} = 35m$.

Two heuristic methods: FollowerStopper and PI with Saturation. The following description of FollowerStopper and PI with Saturation resembles the motivation in [19]. Specifically, the control law of FollowerStopper is

$$v^{\mathrm{cmd}} = \begin{cases} 0, & \text{if } \Delta x \le \Delta x_1, \\ v\dfrac{\Delta x - \Delta x_1}{\Delta x_2 - \Delta x_1}, & \text{if } \Delta x_1 < \Delta x \le \Delta x_2, \\ v + (U - v)\dfrac{\Delta x - \Delta x_2}{\Delta x_3 - \Delta x_2}, & \text{if } \Delta x_2 < \Delta x \le \Delta x_3, \\ U, & \text{if } \Delta x_3 < \Delta x, \end{cases}$$

where v^{cmd} is the command velocity of the autonomous vehicle; Δx is the spacing; U is the preset desired velocity. In the simulations we set $\Delta x_1 = 12.5m$, $\Delta x_2 = 14.75m$, $\Delta x_3 = 20m$, and v is defined as

$$v = \min\left(\max\left(v^{\mathrm{lead}}, 0\right), U\right),$$

where v^{lead} is the velocity of the leading vehicle. As for the control strategy in the PI with Saturation, the autonomous vehicle estimates the average equilibrium velocity U based on its own history data using the previous m time steps.

$$U = \frac{1}{m}\sum_{j=1}^{m} v(j).$$

The target velocity v^{target} is defined as

$$v^{\mathrm{target}} = U + v^{\mathrm{catch}} \times \min\left(\max\left(\frac{\Delta x - g_{\mathrm{l}}}{g_{\mathrm{u}} - g_{\mathrm{l}}}, 0\right), 1\right),$$

where v^{catch} is the allowed velocity for the vehicle to catch up to its preceding vehicle. In the simulations, we used $v^{\mathrm{catch}} = 1m/s$; $g_{\mathrm{l}} = 7m$ is the lower gap limit; $g_{\mathrm{u}} = 30m$ is the upper gap limit. Then, the command velocity for step $j+1$ is obtained as

$$v^{\mathrm{cmd}}(j+1) = \beta_j\left(\alpha_j v^{\mathrm{target}}(j) + (1-\alpha_j)v_j^{\mathrm{lead}}\right) + (1-\beta_j)v^{\mathrm{cmd}}(j).$$

Then, the following dynamics are used to transform the signal v^{cmd} from FollowerStopper and PI with Saturation into an acceleration signal,

$$\dot{v}(t) = \alpha(v^{\mathrm{cmd}} - v(t)),$$

where we used $\alpha = 0.6$ in the simulations.

In addition, we assume that all the vehicles are equipped with a Safe Distance system, in order to avoid crashes. The specific expression of Safe Distance system is

$$\dot{v}(t) = a_{\min}, \text{ if } \frac{v_i^2 - v_{i-1}^2}{2s_i} \ge |a_{\min}|,$$

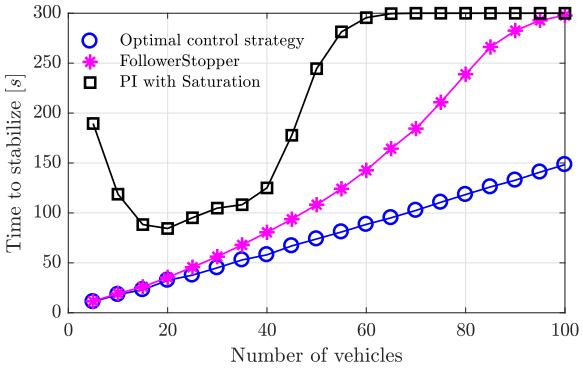

Supplementary Figure S3: Experiment A, time required to smooth the disturbances in the mixed traffic flow. Our optimal control strategy requires the least amount of time to stabilize the mixed traffic flow, and the strategy of PI with Saturation fails to stabilize the mix traffic within 300 seconds when the number of vehicles is larger than 65.

where $a_{\min}$ is the minimum acceleration and $a_{\min} = -5m/s^2$. We assume that there are n vehicles on the ring road, and the spacing of each vehicle at the equilibrium state is fixed to $s^* = 20m$. Then, the circumference is $L = ns^*$ (the length of each vehicle is neglected).

Numerical experiments. In Experiment A, each vehicle has a weak perturbation around its equilibrium state at initial time, in the sense that the position and the velocity of the i-th vehicle are $iL/n + \delta s$, and $v_{\text{ini}} + \delta v$, where v_{ini} is the equilibrium velocity corresponding to the equilibrium spacing L/n, $\delta s \sim U[-4, 4]$ and $\delta v \sim U[-2, 2]$ with $U[a, b]$ denoting a uniform distribution between a and b. In this experiment, we compare the performance of the three methods in different system size n, *i.e.*, the number of vehicles in the mixed traffic flow. As shown in Figure S3, our optimal strategy leads to the best performance in terms of the time required for smoothing the disturbances. The settling time for our method is only around half of that by FollowerStopper, and the strategy of PI with saturation fails to stabilize the traffic flow within 300 seconds when $n \geq 65$.

In Experiment B, we assume that one vehicle has a rapid and strong perturbation. In the beginning, the traffic flow is at the equilibrium state with the velocity $15m/s$. At $t = 20s$, the i-th vehicle decelerates to $5m/s$ in 2 seconds. This situation often happens in the presence of infrastructure bottlenecks or lane changing. Scenarios with different positions of the perturbation are tested, *i.e.*, the perturbed vehicle i can be $2, 3, \ldots, n$. Note that no.1 vehicle is the autonomous vehicle. Simulation results corresponding to the optimal control strategy, FollowerStopper and PI with Saturation, are shown in Figures S4, S5 and S6, respectively. In all the tested scenarios, the perturbation was successfully dampened using the three methods, among which our optimal strategy took the shortest time and the lowest control energy. As shown in Figure S7, this finding holds irrespectively of the position of the perturbation. Furthermore, as shown in Figure S4, we observe that our optimal control strategy is able to reject the perturbation before it propagates around the ring road in one circle . For the other two methods, however, the traffic wave exists for about two propagation periods (see Figures S5 and S6).

Remark 3 (Parameter selection of controllers)**.** *There are many parameters in the strategies of FollowerStopper and PI with Saturation that need to be pre-determined. Different choices of parameter values may lead to different performance, which are not completely predictable. Instead, only three parameters need to be designed in the optimal control strategy, i.e., the weight coefficients in the cost function, γ_s, γ_v, and γ_u. Moreover, we can adjust their values*

to achieve different and predictable results. For example, setting a larger value to γ_s and γ_v typically allows to stabilize the traffic in a shorter time, and setting a larger value to γ_u normally helps to keep a lower control energy for the autonomous vehicle.

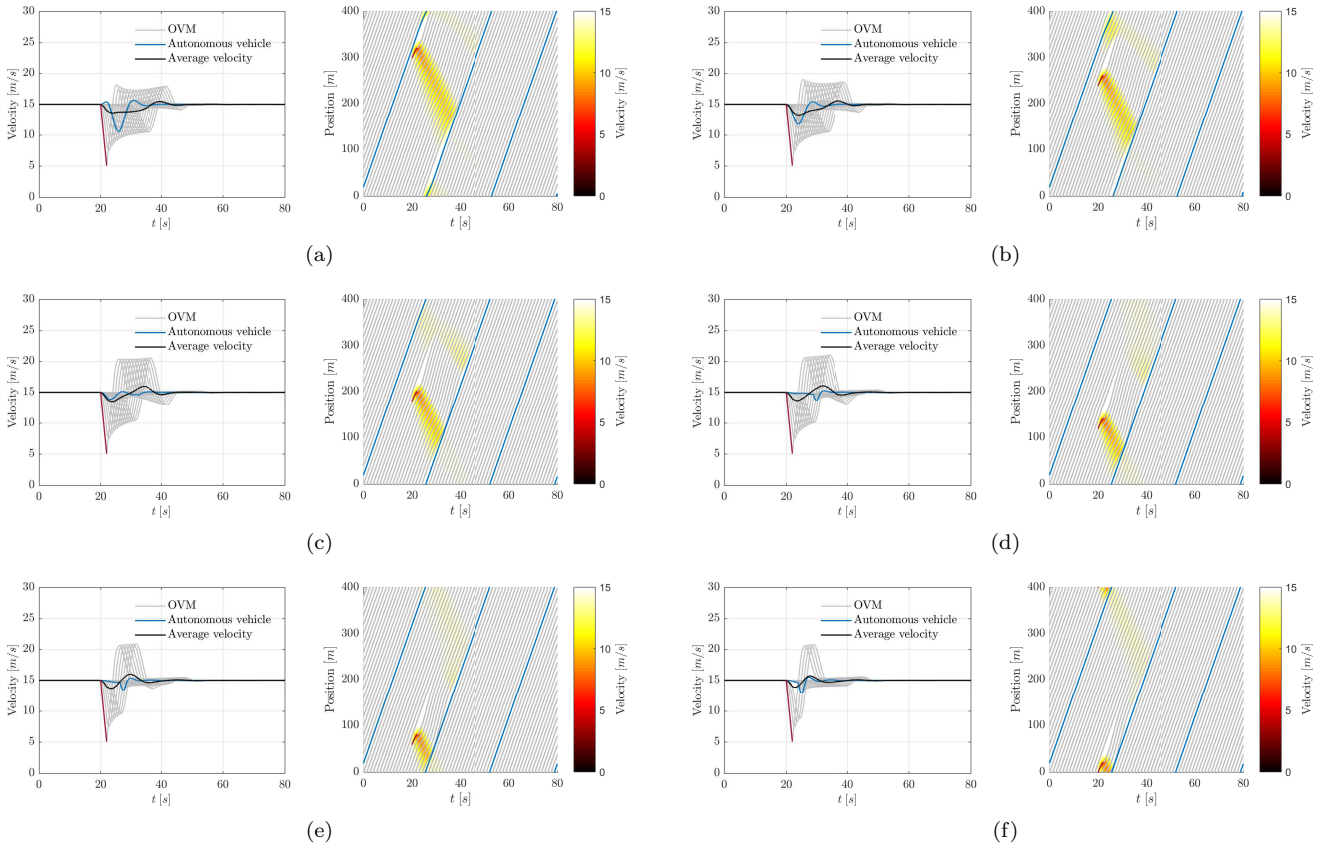

Supplementary Figure S4: Trajectory and velocity profiles of Experiment B where the autonomous vehicle adopts the optimal control strategy. In each subfigure, the left one is the trajectory of each vehicle (human-driven vehicles are grey and the autonomous vehicle is blue). The right one is the velocity of each vehicle. The deeper the color red, the slower the velocity, so the red zone can represent the traffic wave. The red line means the perturbation and the black line is the average velocity of all the vehicles. The index of the autonomous vehicle is 1. (a)-(f) corresponds to the case where the 2^{nd}, 5^{th}, 8^{th}, 11^{th}, 14^{th}, and 17^{th} vehicle is subject to the rapid and strong perturbation, respectively.

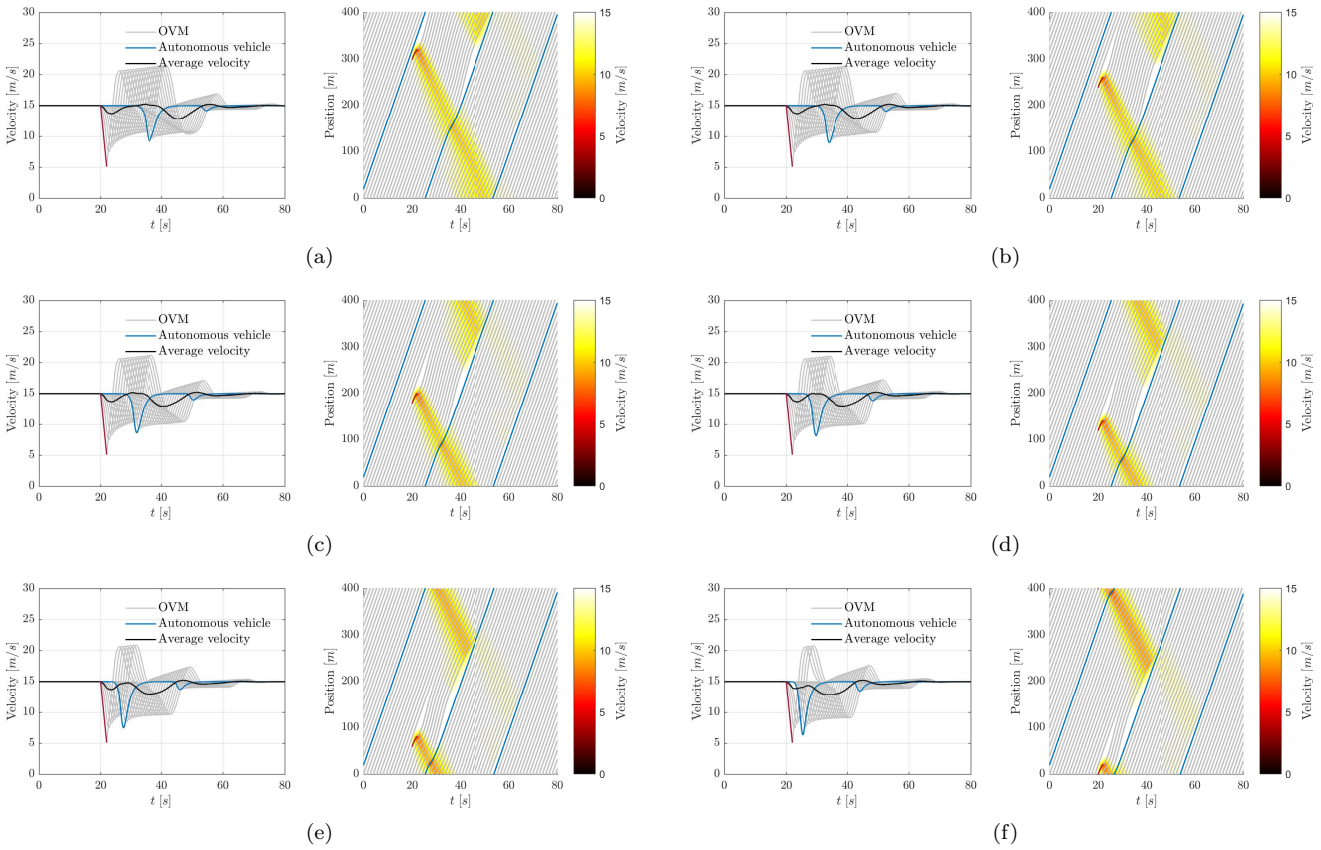

Supplementary Figure S5: Trajectory and velocity profiles of Experiment B where the autonomous vehicle adopts the FollowerStopper strategy. In each subfigure, the left one is the trajectory of each vehicle (human-driven vehicles are grey and the autonomous vehicle is blue). The right one is the velocity of each vehicle. The deeper the color red, the slower the velocity, so the red zone can represent the traffic wave. The red line means the perturbation and the black line is the average velocity of all the vehicles. The index of the autonomous vehicle is 1. (a)-(f) corresponds to the case where the 2^{nd}, 5^{th}, 8^{th}, 11^{th}, 14^{th}, and 17^{th} vehicle is subject to the rapid and strong perturbation, respectively.

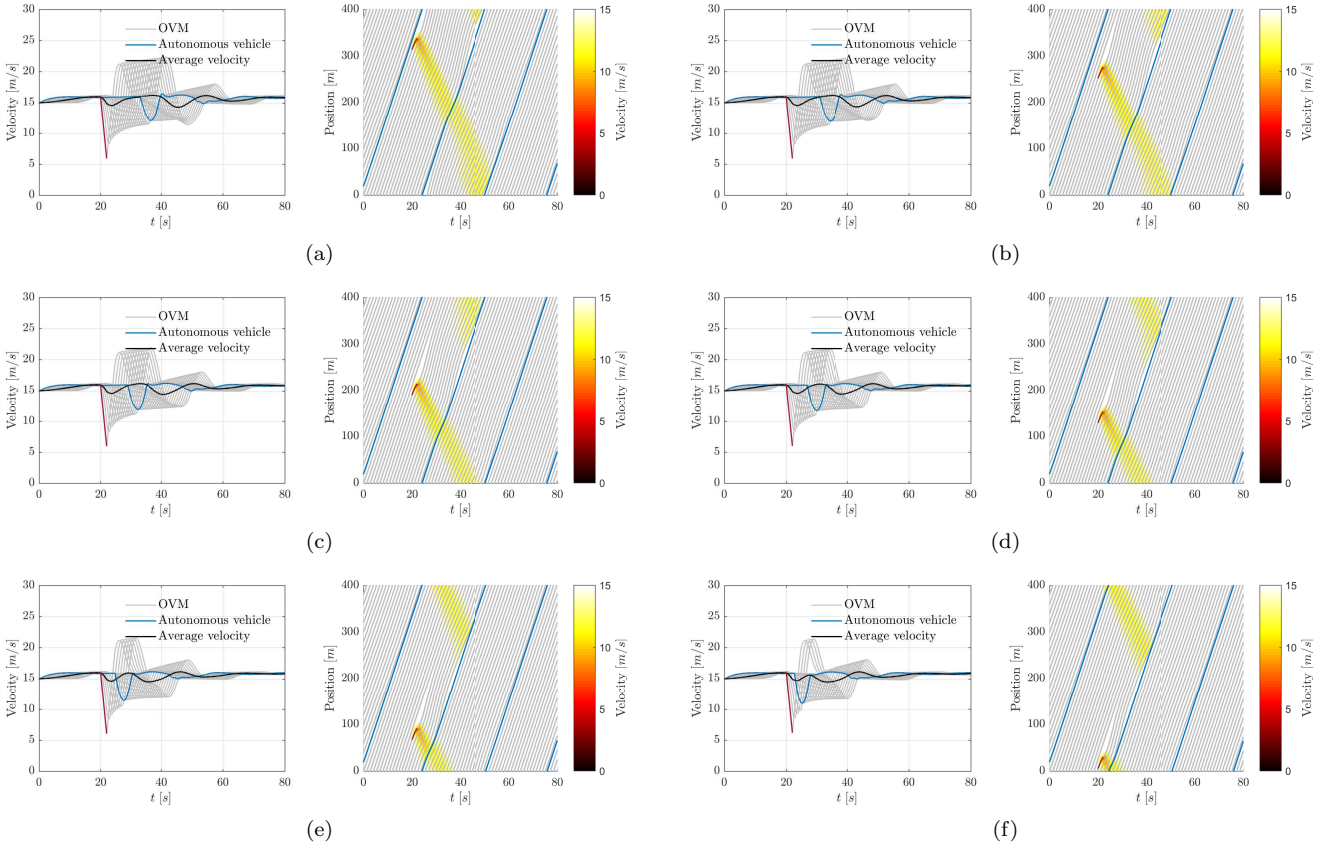

Supplementary Figure S6: Trajectory and velocity profiles of Experiment B where the autonomous vehicle adopts the PI with Saturation strategy. In each subfigure, the left one is the trajectory of each vehicle (human-driven vehicles are grey and the autonomous vehicle is blue). The right one is the velocity of each vehicle. The deeper the color red, the slower the velocity, so the red zone can represent the traffic wave. The red line means the perturbation and the black line is the average velocity of all the vehicles. The index of the autonomous vehicle is 1. (a)-(f) corresponds to the case where the 2^{nd}, 5^{th}, 8^{th}, 11^{th}, 14^{th}, and 17^{th} vehicle is subject to the rapid and strong perturbation, respectively.

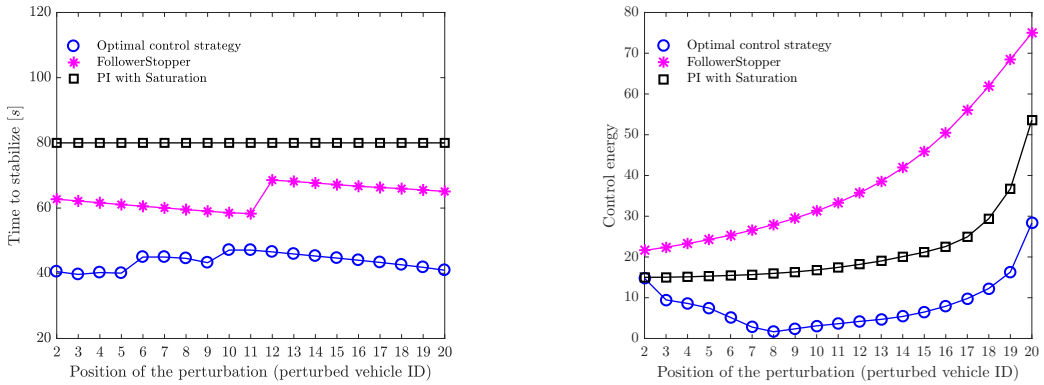

(a) (b)

Supplementary Figure S7: Comparison of results in Experiment B (one vehicle is subject to a rapid and severe perturbation). (a) The time required for the traffic flow to become steady. The perturbation happens at $t = 20s$ and the time length of simulations is 100 seconds, within which PI with Saturation failed to stabilize the traffic, therefore the results for PI with Saturation are presented as 80 seconds. (b) Control energy $\int_0^\infty u(t)^\mathsf{T} u(t) dt$ of the autonomous vehicle.

S6. Mixed traffic systems with multiple autonomous vehicles

In this section, we analyze the mixed traffic system with k autonomous vehicles. The indices of the autonomous vehicles are i_1, i_2, ..., i_k, for which we define a set $S_{\text{AV}} = \{i_1, i_2, \ldots, i_k\}$. The state-space dynamics are given by

$$\dot{x}(t) = A_k x(t) + B_k u(t) = \begin{bmatrix} A_{11} & 0 & \ldots & \ldots & 0 & A_{12} \\ A_{22} & A_{21} & 0 & \ldots & \ldots & 0 \\ 0 & A_{32} & A_{31} & 0 & \ldots & 0 \\ \vdots & \ddots & \ddots & \ddots & \ddots & \vdots \\ 0 & \ldots & 0 & A_{(n-1)2} & A_{(n-1)1} & 0 \\ 0 & \ldots & \ldots & 0 & A_{n2} & A_{n1} \end{bmatrix} x(t) + \begin{bmatrix} P_1, P_2, \ldots, P_k \end{bmatrix} u(t). \tag{S27}$$

In the system matrix A_k, we have

$$\begin{cases} A_{r2} = C_2, A_{r1} = C_1, & \text{if } r \in S_{\text{AV}}, \\ A_{r2} = A_2, A_{r1} = A_1, & \text{if } r \notin S_{\text{AV}}, \end{cases}$$

and the other blocks are zero, where A_1, A_2, C_1 and C_2 are the same as that in (S13). In B_k, each column P_r is a $2n \times 1$ vector, in which only the $(2i_r)$-th entry is 1 and the others are zero. In (S27), the input signal consists of $u(t) = \left[u_{i_1}(t), u_{i_2}(t), \ldots, u_{i_k}(t)\right]^\mathsf{T}$, where $u_{i_r}(t)$ is the control input of the r-th autonomous vehicle, $i_r \in S_{\text{AV}}$.

Similar to Supplementary Note 3, to analyze the system controllability, we first define a virtual control input as

$\hat{u}(t) = u(t) - \left[\alpha_1 \tilde{s}_{i_1}(t) - \alpha_2 \tilde{v}_{i_1}(t) + \alpha_3 \tilde{v}_{i_1-1}(t), \ldots, \alpha_1 \tilde{s}_{i_k}(t) - \alpha_2 \tilde{v}_{i_k}(t) + \alpha_3 \tilde{v}_{i_k-1}(t)\right]^{\mathsf{T}}$. Then (S27) becomes

$$\dot{x}(t) = \begin{bmatrix} A_1 & 0 & \ldots & \ldots & 0 & A_2 \\ A_2 & A_1 & 0 & \ldots & \ldots & 0 \\ 0 & A_2 & A_1 & 0 & \ldots & 0 \\ \vdots & \ddots & \ddots & \ddots & \ddots & \vdots \\ 0 & \ldots & 0 & A_2 & A_1 & 0 \\ 0 & \ldots & \ldots & 0 & A_2 & A_1 \end{bmatrix} x(t) + B_k \hat{u}_k(t) = \hat{A} x(t) + B_k \hat{u}_k(t).$$

Using $F_n^* \otimes I_2$ as the transformation matrix, $(\hat{A}, B_k)$ can be transformed into $(\widetilde{A}, \widetilde{B}_k)$ with $\widetilde{A}$ being the same as (S16) and $\widetilde{B}_k$ defined as

$$\begin{aligned} \widetilde{B}_k &= (F_n^* \otimes I_2)^{-1} B_k = (F_n \otimes I_2) B_k \\ &= \frac{1}{\sqrt{n}} \begin{bmatrix} I_2 & I_2 & I_2 & \cdots & I_2 \\ I_2 & \bar{\omega} I_2 & \bar{\omega}^2 I_2 & \cdots & \bar{\omega}^{n-1} I_2 \\ I_2 & \bar{\omega}^2 I_2 & \bar{\omega}^4 I_2 & \cdots & \bar{\omega}^{2(n-1)} I_2 \\ \vdots & \vdots & \vdots & & \vdots \\ I_2 & \bar{\omega}^{n-1} I_2 & \bar{\omega}^{2(n-1)} I_2 & \cdots & \bar{\omega}^{(n-1)(n-1)} I_2 \end{bmatrix} B_k = \frac{1}{\sqrt{n}} \left[\widetilde{P}_1, \widetilde{P}_2, \ldots, \widetilde{P}_k\right], \end{aligned}$$

where $\widetilde{P}_r = \left[0, 1, 0, \bar{\omega}^{i_r - 1}, \ldots, 0, \bar{\omega}^{(n-1)(i_r-1)}\right]^{\mathsf{T}}, r = 1, \ldots, k$. After the transformation, the new state variable $\tilde{x}$ is the same as (S17). Hence, we have

$$\begin{aligned} \dot{\tilde{x}} &= \widetilde{A} \tilde{x}(t) + \widetilde{B}_k \hat{u}(t) \\ &= \begin{bmatrix} D_1 & & & \\ & D_2 & & \\ & & \ddots & \\ & & & D_n \end{bmatrix} \tilde{x}(t) + \frac{1}{\sqrt{n}} \begin{bmatrix} 0 & 0 & \ldots & 0 \\ 1 & 1 & \ldots & 1 \\ 0 & 0 & \ldots & 0 \\ \bar{\omega}^{i_1 - 1} & \bar{\omega}^{i_2 - 1} & \ldots & \bar{\omega}^{i_k - 1} \\ \vdots & \vdots & \ldots & \vdots \\ 0 & 0 & \ldots & 0 \\ \bar{\omega}^{(n-1)(i_1-1)} & \bar{\omega}^{(n-1)(i_2-1)} & \ldots & \bar{\omega}^{(n-1)(i_k-1)} \end{bmatrix} \hat{u}(t). \end{aligned} \tag{S28}$$

Note that the dynamics (S28) would be reduced to the case with a single autonomous vehicle (S18) when $k = 1$ and $i_1 = 1$. Upon denoting $\tilde{x}(t) = \left[\tilde{x}_{11}, \tilde{x}_{12}, \tilde{x}_{21}, \tilde{x}_{22}, \ldots, \tilde{x}_{n1}, \tilde{x}_{n2}\right]^{\mathsf{T}}$, $(\widetilde{A}, \widetilde{B}_k)$ can be decoupled into n independent

subsystems ($q = 1, 2, \ldots, n$)

$$\begin{aligned}\frac{d}{dt}\begin{bmatrix}\tilde{x}_{q1}\\ \tilde{x}_{q2}\end{bmatrix} &= D_i\begin{bmatrix}\tilde{x}_{q1}\\ \tilde{x}_{q2}\end{bmatrix} + \frac{1}{\sqrt{n}}\begin{bmatrix}0 & 0 & \cdots & 0\\ \bar{\omega}^{(q-1)(i_1-1)} & \bar{\omega}^{(q-1)(i_2-1)} & \ldots & \bar{\omega}^{(q-1)(i_k-1)}\end{bmatrix}\hat{u}(t)\\ &= \begin{bmatrix}0 & -1+\omega^{(n-1)(q-1)}\\ \alpha_1 & -\alpha_2+\alpha_3\omega^{(n-1)(q-1)}\end{bmatrix}\begin{bmatrix}\tilde{x}_{i1}\\ \tilde{x}_{i2}\end{bmatrix} + \frac{1}{\sqrt{n}}\begin{bmatrix}0 & 0 & \cdots & 0\\ \bar{\omega}^{(q-1)(i_1-1)} & \bar{\omega}^{(q-1)(i_2-1)} & \ldots & \bar{\omega}^{(q-1)(i_k-1)}\end{bmatrix}\hat{u}(t).\end{aligned}$$

After some algebraic simplification, the controllability of each sub-system is tested as

$$\begin{aligned}&\operatorname{rank}(Q_{\mathrm{c},q})\\ &= \operatorname{rank}\left(\begin{bmatrix}0 & \cdots & 0 & \left(-1+\omega^{(n-1)(q-1)}\right)\bar{\omega}^{(q-1)(i_1-1)} & \cdots & \left(-1+\omega^{(n-1)(q-1)}\right)\bar{\omega}^{(q-1)(i_k-1)}\\ \bar{\omega}^{(q-1)(i_1-1)} & \ldots & \bar{\omega}^{(q-1)(i_k-1)} & \left(-\alpha_2+\alpha_3\omega^{(n-1)(q-1)}\right)\bar{\omega}^{(q-1)(i_1-1)} & \ldots & \left(-\alpha_2+\alpha_3\omega^{(n-1)(q-1)}\right)\bar{\omega}^{(q-1)(i_k-1)}\end{bmatrix}\right)\\ &= \operatorname{rank}\left(\begin{bmatrix}0 & -1+\omega^{(n-1)(q-1)}\\ 1 & -\alpha_2+\alpha_3\omega^{(n-1)(q-1)}\end{bmatrix}\right), \quad q = 1, 2, \ldots, n.\end{aligned}$$

It is not difficult to see that $\operatorname{rank}(Q_{\mathrm{c},1}) = 1$. In summary, the uncontrollable mode $\tilde{x}_{11}$ still exists, and we have that

$$x_{11} = \frac{1}{\sqrt{n}}\left(\sum_{i\in S_{\mathrm{AV}}}\left(s_i(t) - s^*_{i,\mathrm{c}}\right) + \sum_{i\in\{1,2,\ldots,n\}\backslash S_{\mathrm{AV}}}\left(s_i(t) - s^*\right)\right) \tag{S29}$$

remains constant, where $s^*_{i,\mathrm{c}}$ is the desired spacing of the autonomous vehicle i, $i \in S_{\mathrm{AV}}$. Similar to Supplementary Note 3, there exists an uncontrollable mode corresponding to a zero eigenvalue in the mixed traffic system with multiple autonomous vehicles. Thus, the mixed traffic system (S27) is not completely controllable. One physical interpretation is that the sum of each vehicle's spacing should remain constant due to the ring road structure. Also, the mixed traffic system (S27) is stabilizable since (S12) is stabilizable.

Similar to the reachability analysis, the final state of stable system (S27) can be obtained via

$$\begin{cases}\tilde{v}_i(t_{\mathrm{f}}) = v_{\mathrm{e}}, & i \in \{1, 2, \ldots, n\},\\ \tilde{s}_i(t_{\mathrm{f}}) = \dfrac{\alpha_2 - \alpha_3}{\alpha_1}v_{\mathrm{e}}, & i \in \{1, 2, \ldots, n\}\backslash S_{\mathrm{AV}},\\ \tilde{s}_i(t_{\mathrm{f}}) = s_{\mathrm{e},i}, & i \in S_{\mathrm{AV}}.\end{cases}$$

where v_{e} and $s_{\mathrm{e},i}$, $i \in S_{\mathrm{AV}}$ should satisfy

$$\begin{aligned}\left(\frac{\alpha_2 - \alpha_3}{\alpha_1}\sum_{i\in\{1,2,\ldots,n\}\backslash S_{\mathrm{AV}}} k_{i,1} + \sum_{i\in\{1,2,\ldots,n\}} k_{i,2}\right)v_e + \sum_{i\in S_{\mathrm{AV}}} k_{i,1}s_{\mathrm{e},i} = 0,\\ (n-k)\left(\frac{\alpha_2 - \alpha_3}{\alpha_1}v_{\mathrm{e}} + s^*\right) + \sum_{i\in S_{\mathrm{AV}}}\left(s^*_{i,\mathrm{c}} + s_{\mathrm{e},i}\right) = L.\end{aligned}$$

To reach the desired equilibrium state (s^*, v^*), we should have $v_{\mathrm{e}} = 0$ and $s_{\mathrm{e},i} = 0$, $i \in S_{\mathrm{AV}}$. Together with the

uncontrollable mode (S29), a reachable final state is in the form of $\left[s_{\mathrm{des},1}, v^*, s_{\mathrm{des},2}, v^*, \ldots, s_{\mathrm{des},n}, v^*\right] \in \mathbb{R}^{2n}$, where

$$\begin{cases} s_{\mathrm{des},i} = s^*, & i \in \{1,2,\ldots,n\} \backslash S_{\mathrm{AV}}, \\ s_{\mathrm{des},i} = s^*_{i,\mathrm{c}}, & i \in S_{\mathrm{AV}}. \end{cases}$$

For $s^*_{i,\mathrm{c}},\ i \in S_{\mathrm{AV}}$, they must satisfy $\sum_{i \in S_{\mathrm{AV}}} s^*_{i,c} = L - (n-k)s^*$. This completes our analysis in the scenario with multiple autonomous vehicles.

---

[1] Michael Batty. The size, scale, and shape of cities. *science*, 319(5864):769–771, 2008.

[2] Jonathan I Levy, Jonathan J Buonocore, and Katherine Von Stackelberg. Evaluation of the public health impacts of traffic congestion: a health risk assessment. *Environmental health*, 9(1):65, 2010.

[3] Dirk Helbing. Traffic and related self-driven many-particle systems. *Reviews of modern physics*, 73(4):1067, 2001.

[4] Gábor Orosz, R Eddie Wilson, and Gábor Stépán. Traffic jams: dynamics and control, 2010.

[5] Stef Smulders. Control of freeway traffic flow by variable speed signs. *Transportation Research Part B: Methodological*, 24(2):111–132, 1990.

[6] Markos Papageorgiou, Elias Kosmatopoulos, and Ioannis Papamichail. Effects of variable speed limits on motorway traffic flow. *Transportation Research Record: Journal of the Transportation Research Board*, (2047):37–48, 2008.

[7] Daniel J Fagnant and Kara Kockelman. Preparing a nation for autonomous vehicles: opportunities, barriers and policy recommendations. *Transportation Research Part A: Policy and Practice*, 77:167–181, 2015.

[8] Steven E Shladover, Charles A Desoer, J Karl Hedrick, Masayoshi Tomizuka, Jean Walrand, W-B Zhang, Donn H McMahon, Huei Peng, Shahab Sheikholeslam, and Nick McKeown. Automated vehicle control developments in the path program. *IEEE Transactions on vehicular technology*, 40(1):114–130, 1991.

[9] Shengbo Eben Li, Yang Zheng, Keqiang Li, Yujia Wu, J Karl Hedrick, Feng Gao, and Hongwei Zhang. Dynamical modeling and distributed control of connected and automated vehicles: Challenges and opportunities. *IEEE Intelligent Transportation Systems Magazine*, 9(3):46–58, 2017.

[10] Gerrit JL Naus, Rene PA Vugts, Jeroen Ploeg, Marinus JG van de Molengraft, and Maarten Steinbuch. String-stable cacc design and experimental validation: A frequency-domain approach. *IEEE Transactions on vehicular technology*, 59(9):4268–4279, 2010.

[11] Vicente Milanés, Steven E Shladover, John Spring, Christopher Nowakowski, Hiroshi Kawazoe, and Masahide Nakamura. Cooperative adaptive cruise control in real traffic situations. *IEEE Trans. Intelligent Transportation Systems*, 15(1):296–305, 2014.

[12] Yang Zheng, Shengbo Eben Li, Keqiang Li, Francesco Borrelli, and J Karl Hedrick. Distributed model predictive control for heterogeneous vehicle platoons under unidirectional topologies. *IEEE Transactions on Control Systems Technology*, 25(3):899–910, 2017.

[13] Bart Van Arem, Cornelie JG Van Driel, and Ruben Visser. The impact of cooperative adaptive cruise control on traffic-flow characteristics. *IEEE Transactions on Intelligent Transportation Systems*, 7(4):429–436, 2006.

[14] Steven Shladover, Dongyan Su, and Xiao-Yun Lu. Impacts of cooperative adaptive cruise control on freeway traffic flow. *Transportation Research Record: Journal of the Transportation Research Board*, (2324):63–70, 2012.

[15] Hao Liu, Xingan David Kan, Steven E Shladover, Xiao-Yun Lu, and Robert E Ferlis. Modeling impacts of cooperative adaptive cruise control on mixed traffic flow in multi-lane freeway facilities. *Transportation Research Part C: Emerging*

Technologies, 95:261–279, 2018.

[16] Gábor Orosz. Connected cruise control: modelling, delay effects, and nonlinear behaviour. *Vehicle System Dynamics*, 54(8):1147–1176, 2016.

[17] I Ge Jin and Gábor Orosz. Connected cruise control among human-driven vehicles: Experiment-based parameter estimation and optimal control design. *Transportation Research Part C: Emerging Technologies*, 95:445–459, 2018.

[18] Shumo Cui, Benjamin Seibold, Raphael Stern, and Daniel B Work. Stabilizing traffic flow via a single autonomous vehicle: Possibilities and limitations. In *Intelligent Vehicles Symposium (IV), 2017 IEEE*, pages 1336–1341. IEEE, 2017.

[19] Raphael E Stern, Shumo Cui, Maria Laura Delle Monache, Rahul Bhadani, Matt Bunting, Miles Churchill, Nathaniel Hamilton, Hannah Pohlmann, Fangyu Wu, Benedetto Piccoli, et al. Dissipation of stop-and-go waves via control of autonomous vehicles: Field experiments. *Transportation Research Part C: Emerging Technologies*, 89:205–221, 2018.

[20] Ryosuke Nishi, Akiyasu Tomoeda, Kenichiro Shimura, and Katsuhiro Nishinari. Theory of jam-absorption driving. *Transportation Research Part B: Methodological*, 50:116–129, 2013.

[21] Cathy Wu, Aboudy Kreidieh, Kanaad Parvate, Eugene Vinitsky, and Alexandre M Bayen. Flow: Architecture and benchmarking for reinforcement learning in traffic control. *arXiv preprint arXiv:1710.05465*, 2017.

[22] Cathy Wu, Aboudy Kreidieh, Eugene Vinitsky, and Alexandre M Bayen. Emergent behaviors in mixed-autonomy traffic. In *Conference on Robot Learning*, pages 398–407, 2017.

[23] Yuki Sugiyama, Minoru Fukui, Macoto Kikuchi, Katsuya Hasebe, Akihiro Nakayama, Katsuhiro Nishinari, Shin-ichi Tadaki, and Satoshi Yukawa. Traffic jams without bottlenecksexperimental evidence for the physical mechanism of the formation of a jam. *New journal of physics*, 10(3):033001, 2008.

[24] John Toner and Yuhai Tu. Flocks, herds, and schools: A quantitative theory of flocking. *Physical review E*, 58(4):4828, 1998.

[25] Ali Jadbabaie, Jie Lin, and A Stephen Morse. Coordination of groups of mobile autonomous agents using nearest neighbor rules. *IEEE Transactions on automatic control*, 48(6):988–1001, 2003.

[26] Yang-Yu Liu, Jean-Jacques Slotine, and Albert-László Barabási. Controllability of complex networks. *Nature*, 473(7346):167, 2011.

[27] Jean-Jacques E Slotine, Weiping Li, et al. *Applied nonlinear control*, volume 199. Prentice hall Englewood Cliffs, NJ, 1991.

[28] Brian J Olson, Steven W Shaw, Chengzhi Shi, Christophe Pierre, and Robert G Parker. Circulant matrices and their application to vibration analysis. *Applied Mechanics Reviews*, 66(4):040803, 2014.

[29] Joshua A Marshall, Mireille E Broucke, and Bruce A Francis. Formations of vehicles in cyclic pursuit. *IEEE Transactions on automatic control*, 49(11):1963–1974, 2004.

[30] Masako Bando, Katsuya Hasebe, Akihiro Nakayama, Akihiro Shibata, and Yuki Sugiyama. Dynamical model of traffic congestion and numerical simulation. *Physical review E*, 51(2):1035, 1995.

[31] Sigurd Skogestad and Ian Postlethwaite. *Multivariable feedback control: analysis and design*, volume 2. Wiley New York, 2007.

[32] Yang Zheng, Richard P Mason, and Antonis Papachristodoulou. Scalable design of structured controllers using chordal decomposition. *IEEE Transactions on Automatic Control*, 63(3):752–767, 2018.

[33] Mihailo R Jovanović and Neil K Dhingra. Controller architectures: Tradeoffs between performance and structure. *European Journal of Control*, 30:76–91, 2016.

[34] Mario Di Bernardo, Alessandro Salvi, and Stefania Santini. Distributed consensus strategy for platooning of vehicles in the presence of time-varying heterogeneous communication delays. *IEEE Transactions on Intelligent Transportation Systems*, 16(1):102–112, 2015.

[35] Feng Gao, Shengbo Eben Li, Yang Zheng, and Dongsuk Kum. Robust control of heterogeneous vehicular platoon with uncertain dynamics and communication delay. *IET Intelligent Transport Systems*, 10(7):503–513, 2016.

[36] I Ge Jin and Gábor Orosz. Optimal control of connected vehicle systems with communication delay and driver reaction time. *IEEE Transactions on Intelligent Transportation Systems*, 18(8):2056–2070, 2017.

[37] APS Mosek. The mosek optimization software. *Online at http://www. mosek. com*, 54(2-1):5, 2010.

[38] Martin Treiber, Arne Kesting, and Dirk Helbing. Delays, inaccuracies and anticipation in microscopic traffic models. *Physica A: Statistical Mechanics and its Applications*, 360(1):71–88, 2006.

[39] Robert B Burckel. *An introduction to classical complex analysis*, volume 1. Academic Press, 1980.

[40] Rudolf Emil Kalman. Mathematical description of linear dynamical systems. *Journal of the Society for Industrial and Applied Mathematics, Series A: Control*, 1(2):152–192, 1963.